INL/RPT-23-XXXXX Rev. 001

Lower-length-scale modeling of chemical additions, corrosion and fission products in select MSR base salts

September 30, 2023

Technical Report

Chao Jiang[1], David Andersson[2], Gaoxue Wang[2], Bo Li[2], and Ping Yang[2]

[1]Idaho National Laboratory
[2]Los Alamos National Laboratory

Idaho National Laboratory

INL is a U.S. Department of Energy National Laboratory operated by Batelle Energy Alliance, LLC

Lower-length-scale modeling of chemical additions, corrosion and fission products in select MSR base salts

Technical Report

Chao Jiang[1], David Andersson[2], Gaoxue Wang[2], Bo Li[2], and Ping Yang[2]

[1]Idaho National Laboratory
[2]Los Alamos National Laboratory

September 30, 2023

Idaho National Laboratory
Computational Mechanics and Materials Department
Idaho Falls, Idaho 83415

http://www.inl.gov

Prepared for the
U.S. Department of Energy
Office of Nuclear Energy
Under U.S. Department of Energy-Idaho Operations Office
Contract DE-AC07-05ID14517

Page intentionally left blank

Abstract

Molten salts play a crucial role in advancing Generation IV nuclear energy technology, with chloride-based salts like NaCl-UCl_3 garnering significant attention due to their distinctive properties. However, the corrosive nature of molten salts causes the dissolution of chromium (Cr), leading to the formation of $CrCl_2$ and $CrCl_3$ species in molten chlorides. Moreover, the radioactive decay of nuclear fuel gives rise to fission products, including Cs, Sr, and I chlorides. The first part of this report presents a comprehensive study utilizing ab initio molecular dynamics (AIMD) simulations to investigate the properties of eutectic NaCl-UCl_3 molten salt in the presence of corrosion products ($CrCl_2$ and $CrCl_3$) and fission product (CsCl). The study focuses on essential structural and thermophysical properties such as density, mixing energy, coordination numbers (CN), and Radial Distribution Functions (RDF) of the salts with varying compositions of corrosion products and fission product, covering a range from 0% to 13.5%. The results offer valuable insights into the behavior of corrosion and fission products in uranium-based molten salts, providing essential data that can be used as input to the MTDB-TC and MSTDB-TP property databases being developed by the NEAMS program.

Due to their favorable characteristics such as low melting points, high boiling points, and low costs, $MgCl_2$+NaCl+KCl (MNK) eutectic salts have recently attracted attention as high-temperature heat transfer fluids. The incorporation of LiCl into MNK salts can further reduce their melting points and increase their specific heat capacities, which is desirable for high-temperature heat transfer applications. The second part of this report presents the development and validation of a new shell-model potential for the $MgCl_2$+NaCl+KCl+LiCl system, which captures the polarization of Cl anions. The extensive comparison with experimental data and AIMD simulations demonstrates the accuracy and reliability of the potential. Furthermore, using this potential, we elucidate the intricate network structure in MNK eutectic salts that is formed through polyhedron sharing. This research contributes to a fundamental understanding of the atomic structures and thermophysical properties of multi-component molten salts, which is crucial for future development of heat transfer fluids for applications in molten salt reactors.

Page intentionally left blank

Acknowledgments

This work was fully sponsored by the U.S. Department of Energy, Office of Nuclear Energy, Nuclear Energy Advanced Modeling and Simulation (NEAMS) Program at Idaho National Laboratory operated by Battelle Energy Alliance (BEA) under DOE-NE Idaho Operations Office Contract DE-AC07–05ID14517. Los Alamos National Laboratory, an affirmative action/equal opportunity employer, is operated by Triad National Security, LLC, for the National Nuclear Security Administration of the U.S. Department of Energy under Contract No. 89233218CNA000001. This research made use of the resources of the High Performance Computing Center at Idaho National Laboratory, which is supported by the Office of Nuclear Energy of the U.S. Department of Energy and the Nuclear Science User Facilities under Contract No. DE-AC07-05ID14517. This research also used resources provided by the Los Alamos National Laboratory Institutional Computing Program.

Page intentionally left blank

Contents

List of Figures

List of Tables

1. INTRODUCTION

Molten Salt Reactor (MSRs) has garnered significant attention as a promising candidate for Generation IV nuclear energy systems, owing to their superior safety and efficiency compared to pressurized water reactors [1]. In MSR technology, molten halides are commonly employed as both nuclear fuels and coolants. Molten fluorides such as LiF-BeF_2-ZrF_4 have been traditionally used since the early days of MSR technology in the 1960s for their advantageous properties of high stability, low vapor pressure, and low neutron-capture cross section [2, 3]. On the other hand, molten chlorides are considered by the new generation of fast-spectrum MSR design for their lower viscosity and higher actinide solubility than the fluoride counterparts [4]. The deployment of a fast-spectrum MSR allows spent nuclear fuel as potential fissile materials and therefore lower operational costs [5].

The design of MSRs necessitates a comprehensive understanding of temperature- and composition-dependent thermophysical properties such as density, heat capacity, and viscosity for both the fuel and coolant salts. However, the corrosive nature of molten salts makes experimental measurement of their high-temperature thermophysical properties a formidable challenge. Therefore, the adoption of lower-length-scale modeling techniques becomes imperative to bridge this critical knowledge gap.

The objective of this project is to utilize both ab initio molecular dynamics (AIMD) and classical molecular dynamics (MD) simulations as cost-effective alternatives to experiments for obtaining essential thermophysical properties (such as density, heat capacity, and viscosity) and thermodynamic properties (such as enthalpy of mixing) of molten salts. A particular emphasis is on understanding the effects of chemical additives, corrosion products, and fission products on these properties. Sodium chloride (NaCl) has emerged as the primary choice for dissolving nuclear fuel, such as UCl_3. Additional dilutant chlorides like KCl, LiCl or $MgCl_2$ are often employed to adjust the melting temperature and viscosity of the mixtures. The binary eutectic NaCl-UCl_3 has been established as an acceptable surrogate model of molten chloride fuel system for MSR applications [5]. Furthermore, $MgCl_2$-NaCl-KCl (MNK) eutectic salts have attracted attention as high-temperature heat transfer fluids due to their favorable characteristics such as low melting points and high boiling points [6, 7, 8]. Both molten salt systems, NaCl-UCl_3 and MNK, are the focus of this project in fiscal year 2023 (FY23). Our results are reported in Chapters 2 and 3, respectively.

2. PREDICTION OF THE INFLUENCE OF CORROSION AND FISSION PRODUCTS ON THE PROPERTIES OF URANIUM CHLORIDE BASED FUEL SALTS

The corrosive nature of molten salts poses challenges as it results in the dissolution of elements from functional materials. Cr element is routinely used in structural alloys for molten salt reactors [9], but it exhibits a higher propensity to oxidize and dissolve in the salt melts compared to other common elements in structural materials (like Fe, Ni, and Mo) [10, 11]. Molten chlorides generally show enhanced corrosion rates in comparison to molten fluorides, primarily due to their lower electrochemical potentials [5]. Moreover, chlorides show more complex corrosion behaviors since chlorine can exhibit several oxidation states (+7, +5, +3, 1), leading to intricate bonding configurations and corrosion chemistry. The dissolution of Cr in molten chlorides gives rise to the formation of Cr chloride species, such as $CrCl_2$ and $CrCl_3$, whose concentration is expected to increase steadily during MSR operation. Understanding the behavior of corrosion products in NaCl-UCl_3 and their impact on the thermophysical properties of NaCl-UCl_3 is crucial for effective corrosion control and optimal MSR design. Additionally, the radioactive decay of nuclear fuel leads to the formation of fission products in molten fuel systems. Cs, Sr, I and Xe are some of the common fission products of the U fuel cycle. To the best of our knowledge, there have been no reports on the structural and thermophysical properties of NaCl-UCl_3 with the presence of these corrosion products and fission products.

In this study, we performed AIMD simulations to investigate the behavior of eutectic NaCl-UCl_3 molten salt with the presence of corrosion products $CrCl_2$ and $CrCl_3$, along with the fission product CsCl, up to a molar fraction of 13.5%. Although AIMD simulations are computationally expensive, they represent the gold-standard for benchmarking faster simulation methods like classical force fields for molten salts. Our focus was on analyzing thermophysical properties, such as density, heat capacity, and mixing energy, which can be derived from relatively short simulations of small systems. To gain insight into the behavior of corrosion products in chloride fuels for MSR applications, we performed analyses on the local structure of the mixtures using coordination numbers and Radial Distribution Functions (RDFs). The results obtained from these simulations provide valuable insights into the behavior of corrosion products and fission products in NaCl-UCl_3 molten salt for MSR applications, which are important to advance the ongoing efforts towards optimizing MSR design and corrosion control to ensure the safe and efficient generation of nuclear energy.

2.1 Computational methodology

We performed AIMD simulations using the Vienna ab initio simulation package (VASP) [12, 13] based on density functional theory (DFT) and the Born-Oppenheimer approximation with periodic boundary conditions. The interaction between the electrons and the nucleus was described by the projector augmented wave (PAW) method [14], and the Perdew-Burke-Ernzerhof (PBE)[15] functional of the generalized gradient approximation (GGA) was used for the electron exchangecorrelation. Standard PAW-PBE pseudopotentials were used for Na ($3s^1$), Cl ($3s^2 3p^5$), U ($6s^2 6p^6 5f^2 6d^2 7s^2$), and Cr ($3p^6 3d^5 4s^1$), with a kinetic energy cutoff of 400 eV for the plane wave bases. The Brillouin zone was sampled with a single Γ k-point. A Hubbard U correction [16, 17] was included for the 5f orbitals of U ions and 3d orbitals of Cr ions to capture the strong electron correlation effects. The simplified (rotationally invariant) approach of the DFT+U, introduced by Dudarev [18, 19], was used for the Hubbard U methodology. The U value was 4.0 eV and 3.0 eV for U and Cr, respectively, as suggested by previous studies [2, 20, 21]. The DFT-dDsC dispersion correction [22, 23] was employed since it yields the best agreement with the experimental densities of NaCl and UCl_3 molten salts as demonstrated by our previous studies [20]. DFT-dDsC method does not include parameters for f elements in the standard VASP version. In order to enable simulations for f elements with the dDsC method, the model parameters were taken from Refs. [24] (U: C6=4.889 au, r0=6.416 au) and [25] (U: α= 129.0 au). The convergence criteria for the electronic minimization was 5×10^{-3} eV for all the salts.

The AIMD simulation was carried out in the NPT ensemble with the Langevin thermostat [26]. The simulation temperature ranged from 1000 K to 1200 K, which is higher than the measured melting points of the NaCl-UCl_3 molten salts [27, 28]. The total simulation time for each system was about 50 ps with a time step of 1 fs. The first 20 ps was used to equilibrate the system, and the last 30 ps was used for property analysis. Such time scale was typical of AIMD simulations [2, 20]. We have demonstrated that the density, heat capacity and local structure including RDF of UCl_3 and NaCl molten salts can be accurately described using simulations with such timescale and size [2, 20]. The simulations supercells consist of 22 (NaCl) and 10 (UCl_3), close to its eutectic composition (x=31.25%, where x is the molar composition of UCl_3) [27, 28]. Different numbers of $CrCl_2$/$CrCl_3$/CsCl units from 0 to 5 were added in the NaCl-UCl_3 system, corresponding to Cr mole fraction of 0.0%, 3.0%, 5.8% and 8.6%, 11.1% and 13.5%, respectively. The composition and the size of the simulation units are summarized in Table 2.1. The initial structures were generated using PACKMOL [29].

Table 2.1. Composition and size of the simulation structures for the binary NaCl-UCl_3-$CrCl_2$/$CrCl_3$/CsCl mixtures.

Fraction	0.0%	3.0%	5.9%	8.6%	11.1%	13.5%
# of $CrCl_2$/$CrCl_3$/CsCl units	0	1	2	3	4	5
# of NaCl units	22	22	22	22	22	22
# of UCl_3 units	10	10	10	10	10	10

2.2 Results and discussion

2.2.1 Eutectic NaCl-UCl_3 molten salt

Table 2.2 presents the calculated density of the eutectic NaCl-UCl_3 as function of temperature. Our calculated results show excellent agreement with the experimental value obtained by Desyatnik et al. [30], with a difference of less than 5%. Each U ion in the eutectic exhibit a magnetic moment of approximately 3.0 μB, indicating an oxidation state of +3 for each U ion. Regarding the coordination numbers of U ions, approximately 50% of them have a coordination number of 7 with chlorine atoms, around 30% have a coordination number of 6, and approximately 20% have a coordination number of 5. For a more comprehensive understanding of the thermodynamic properties of binary NaCl-UCl_3 mixtures, detailed information is available in our previously published papers [20, 31].

Table 2.2. Comparison of the calculated and experimental temperature dependence of density of eutectic NaCl-UCl_3 (UCl_3 molar concentration of 31.25%).

	Density (g/cm^3)
Experiment [30]	ρ=3.7598 - 0.8012/1000*T
AIMD	ρ=3.8682 - 0.7792/1000*T

2.2.2 Pure $CrCl_2$ and $CrCl_2$ in eutectic NaCl-UCl_3 molten salt

Figure 2.1 illustrates the structure and density of pure $CrCl_2$ molten salt from our AIMD simulations. At 1000 K, the simulated density of $CrCl_2$ is 2.42 g/cm^3, and it decreases to 2.30 g/cm^3 at 1200 K. The coordination numbers of Cr ions with chlorine atoms are as follows: around 55% have a coordination number of 5, 27% have a coordination number of 6, and 16% have a coordination number of 4. The Cr-Cl bond distance is $\sim$ 2.4 Å, evident from the first peak of the Cr-Cl RDF in Figure 2.1(c). Each Cr ion exhibits a magnetic moment of $\sim$ 3.8 μB, consistent with its oxidation state of +2. Regrettably, no available experimental data for $CrCl_2$ molten salt is currently available to compare with our simulations.

Moving to Figure 2.2(a), it shows the total energy of NaCl-UCl_3-$CrCl_2$ mixture as a function of temperature. We observe that the energy varies linearly with temperature. From the slope of the total energy, we can calculate the constant pressure heat capacity of these molten salts, denoted as $C_p = \left(\frac{\partial E}{\partial T}\right)_p$ [20]. The calculated heat capacity of eutectic NaCl-UCl_3 is 93 J/mol/K. The calculated heat capacity of $CrCl_2$ is 120 J/mol/K. For the NaCl-UCl_3-$CrCl_2$ mixture, its heat capacity is approximately a linear combination of the heat capacity of eutectic NaCl-UCl_3 plus pure $CrCl_2$ as seen in Figure 2.3.

Figure 2.2(b) presents the mixing energies associated with adding $CrCl_2$ to the eutectic NaCl-UCl_3. These mixing energies were determined by calculating the total energy difference between the NaCl-UCl_3-$CrCl_2$ mixture ($E_{NaCl-UCl_3-x(CrCl_2)}$) and the ideal solution (E_{ideal}) at the same temperature using the formula:

$$E_{mixing} = \frac{E_{NaCl-UCl_3-x(CrCl_2)} - E_{ideal}}{N} \tag{2.1}$$

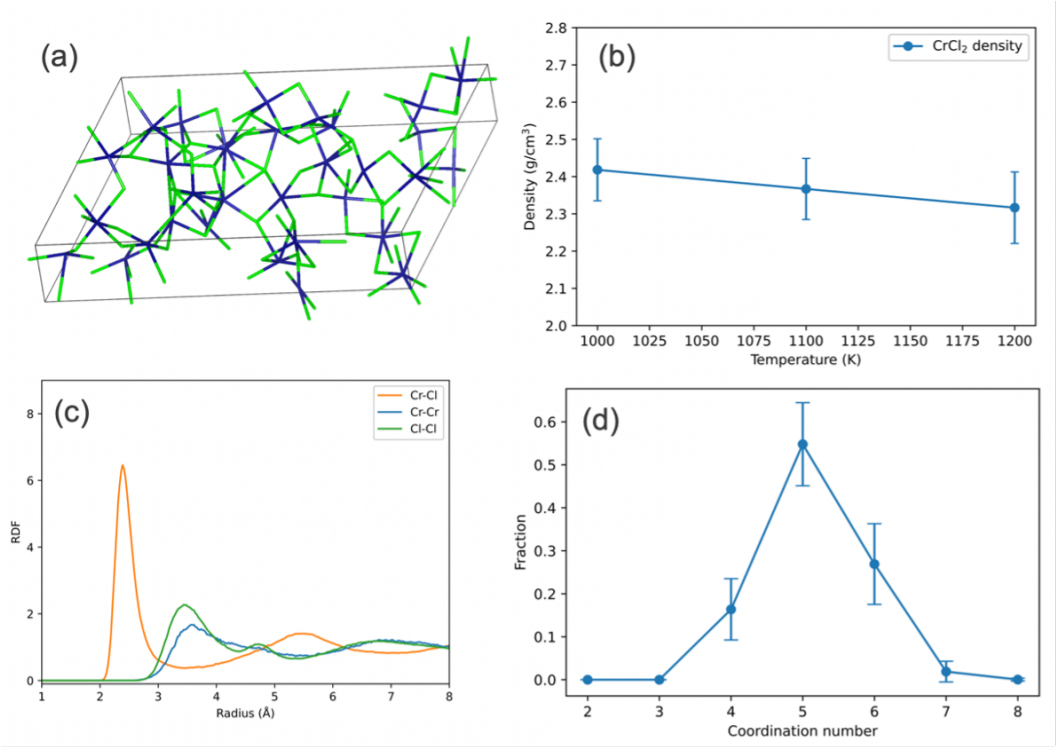

Figure 2.1. Pure $CrCl_2$ molten salts. (a) Snapshot of AIMD trajectories at 1100 K, (b) density at different temperatures, (c) RDF, and (d) Cr coordination number. The error bars show the standard deviation of density or the fraction of coordination number.

where $E_{ideal} = E_{NaCl-UCl_3} + xE_{CrCl_2}$, with x representing the number of $CrCl_2$ units in the system, and N being the number of total atoms. $E_{NaCl-UCl_3}$ refers to the total energy of eutectic NaCl-UCl_3, and E_{CrCl_2} is the total energy of pure $CrCl_2$ molten salt. This definition of mixing energy clarifies the preference of $CrCl_2$ dissolution in eutectic NaCl-UCl_3 molten salt. A negative mixing energy indicates the preference for the formation of $CrCl_2$ corrosion products in the salt, whereas a positive mixing energy suggests that $CrCl_2$ does not favor dissolution in the eutectic NaCl-UCl_3. All NaCl-UCl_3-$CrCl_2$ mixtures exhibit a notable negative mixing energy from our AIMD simulations. The mixing energy decreases to -0.02 eV/atom when the $CrCl_2$ fraction reaches 13.5%, indicating that $CrCl_2$ can thermodynamically dissolve in NaCl-UCl_3 mixture. The calculated mixing energy remains insensitive to changes in temperature as evidenced by the overlapping of the mixing energies under different temperatures.

In Figure 2.2(c), we present the densities of NaCl-UCl_3-$CrCl_2$ from AIMD simulations. Additionally, the density of NaCl-UCl_3 as a function of temperature is provided in Table 2.3. For all the systems considered, the densities exhibit a linear decrease with increasing temperature. Upon incorporating $CrCl_2$ up to a mole concentration of 13.5%, the densities of the systems show a slight decrease compared to the eutectic NaCl-UCl_3.

Figure 2.2(d) shows the simulated density deviation, defined as $\frac{\rho}{\rho_{ideal}}$, where ρ represents the density of the mixture, and ρ_{ideal} is the density of the ideal mixture at the same temperature. The ideal mixture is referenced to the eutectic

$NaCl\text{-}UCl_3$ and pure $CrCl_2$ molten salts. Our simulations consistently indicate a clear positive density deviation for all the mixtures. The magnitude of the density deviation remains within 2% for $CrCl_2$ fractions up to 13.5%. This positive density deviation implies that the structures of $NaCl\text{-}UCl_3\text{-}CrCl_2$ mixtures are more compact compared to eutectic $NaCl\text{-}UCl_3$ and pure $CrCl_2$ molten salts. It is important to note that achieving high accuracy in the density of the mixtures within one percent of the absolute density using AIMD simulations presents challenges [20]. As a result, there are some scatters in the density deviation plot shown in Figure 2.2(d).

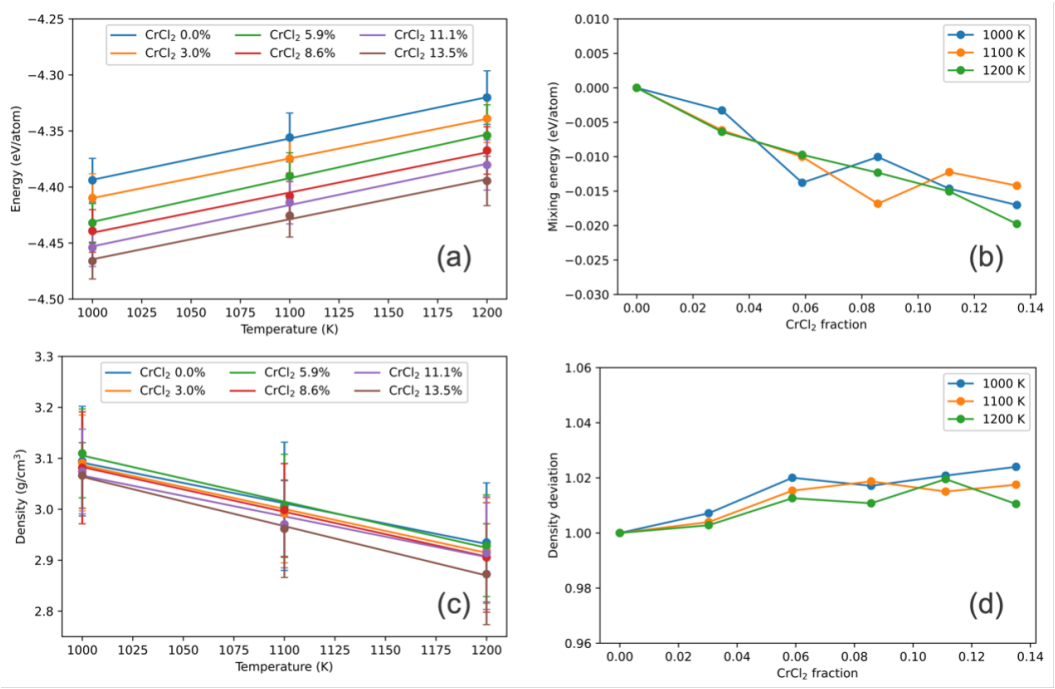

Figure 2.2. (a) Total energy as a function of temperature, (b) mixing energy, (c) density, and (d) density deviation of $NaCl\text{-}UCl_3\text{-}CrCl_2$ mixtures. The error bar shows the standard deviation of energy and density from AIMD simulations.

Table 2.3. Temperature dependence of simulated densities of $NaCl\text{-}UCl_3\text{-}CrCl_2$ mixtures with different $CrCl_2$ mole fraction. The temperature is ranging from 1000 to 1200 K.

$CrCl_2$ fraction	Density (g/cm^3)
0%	ρ=3.8682 - 0.7792/1000*T
3.0%	ρ=3.9482 - 0.8615/1000*T
5.9%	ρ=4.0118 - 0.9062/1000*T
8.6%	ρ=3.9625 - 0.8794/1000*T
11.1%	ρ=3.8672 - 0.8009/1000*T
13.5%	ρ=4.0329 - 0.9691/1000*T

The structural characteristics, RDF and coordination number of Cr and U in $NaCl\text{-}UCl_3\text{-}CrCl_2$ mixtures are presented in Figure 2.4. In these mixtures, Cr exhibits predominantly 5-fold coordination, followed by 6-fold and 4-fold

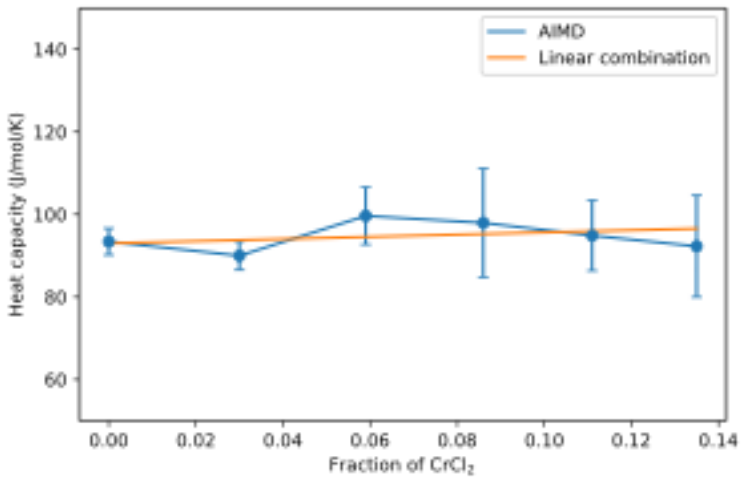

Figure 2.3. Calculated heat capacity of NaCl-UCl_3-$CrCl_2$ mixtures. The blue lines are calculated from slope of total energy of NaCl-UCl_3-$CrCl_2$. The orange line is estimated using a linear combination of the heat capacity of NaCl-UCl_3 and pure $CrCl_2$. The error bars are estimated from the slopes of energy in temperature range of 1000 to 1100K, and 1100 to 1200 K.

coordination, similar to the coordination numbers observed in pure $CrCl_2$. On the other hand, U atoms mainly adopt a 7-fold coordination with Cl, with noteworthy occurrences of 8-fold and 6-fold coordinated structures. Importantly, the coordination of U and Cr remains nearly unchanged with the addition of $CrCl_2$ in eutectic NaCl-UCl_3 within the concentration range studied in this work.

In our previous publications [20, 31], it was demonstrated that a U network structure begins to form in NaCl-UCl_3 with UCl_3 fraction near the eutectic composition. Upon adding $CrCl_2$, it is observed that the Cr complexes become connected to the U network, as depicted in Figure 2.4(a). This connection results in a distinct U-Cr peak at approximated 4.2 Å in the RDF plots, as shown in Figure 2.4(b). The bond lengths of U-Cl and Cr-Cl are approximately 2.8 Å and 2.4 Å, respectively. Overall, the structural analysis reveals that the addition of $CrCl_2$ does not significantly alter the coordination environment of U in the studied concentration range, and the formation of U-Cr complexes plays a crucial role in the network structure of the mixtures. Further investigations are needed to explore the impact of $CrCl_2$ on the transport properties, including diffusivity and viscosity, of NaCl-UCl_3.

2.2.3 Pure $CrCl_3$ and $CrCl_3$ in eutectic NaCl-UCl_3

In Figure 2.5(a), we present the representative energy and volume evolution of $CrCl_3$ obtained from AIMD simulations. It becomes apparent that even after running the simulations for 120 ps, neither the energy nor the volume of the system reaches equilibrium. We have conducted simulations using various initial structures for $CrCl_3$, but all of them exhibit similar behavior. Notably, the system's volume keeps expanding, while chain-like structures start to form, as illustrated in Figures 2.5(b) and 2.5(c).

The challenge in achieving equilibration for $CrCl_3$ arises from the coordination chemistry of Cr^{3+}. In contrast to

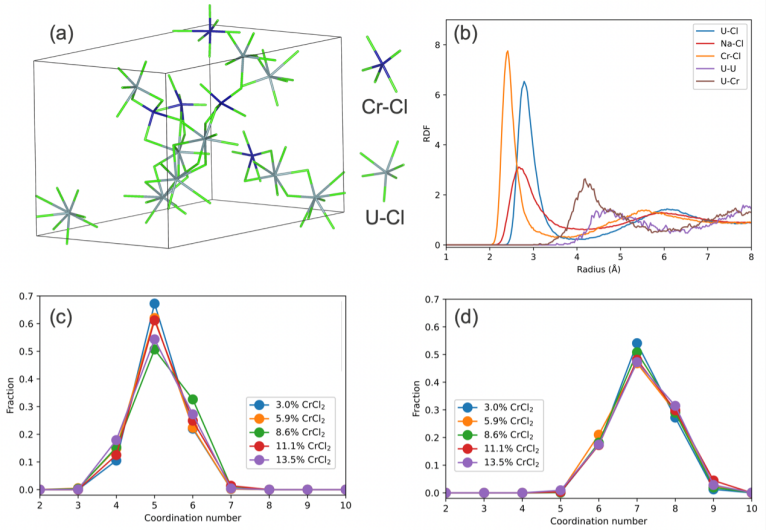

Figure 2.4. (a) Snapshot of AIMD trajectories of NaCl-UCl_3-$CrCl_2$ mixture at 1100 K, (b) RDF of U-Cl (blue), Na-Cl (red), Na-Cl (blue), U-U (purple), and U-Cr (brown) pairs, (c) the fraction of Cr-Cl coordination number, and (d) the fraction of U coordination number. The Na cations are neglected to better visualize the network structure in (a).

pure $CrCl_2$ as shown in Figure 2.1, where the dominant coordination number for Cr^{2+} is 5, followed by coordination number of 4 and 6, the $CrCl_3$ system requires each Cr^{3+} ion to possess a coordination number of 6 to accommodate the additional Cl atoms compared to the pure $CrCl_2$ system. The stable configuration of 6-fold coordinated Cr can manifest as chain structures, as depicted in Figure 2.5(c), or adopt layered structures similar to those observed in bulk $CrCl_3$ [21]. Consequently, reaching relaxation into these specific configurations demands an extended simulation time.

Equilibrating $CrCl_3$ system poses another challenge due to a chemical reaction involving $2CrCl_3 = 2CrCl_2 + Cl_2$. During AIMD simulations of $CrCl_3$, we observed the formation of Cl_2 molecules, resulting in a mixed system of $CrCl_3$-$CrCl_2$-Cl_2 instead of pure $CrCl_3$. Furthermore, we noticed that a larger Hubbard U parameter promotes the formation of more Cl_2, indicating a reduced energy barrier for this chemical reaction with an increased U parameter. As a result of these complexities, accurately modeling the properties of pure $CrCl_3$ molten salt using AIMD simulations proves to be more time-consuming due to the necessity of establishing stable 6-fold coordination of Cr^{3+} ions and the formation of specific structural arrangements, such as chain structures. Further investigation and longer simulation times are needed to fully understand and characterize the behavior of $CrCl_3$.

In the context of $CrCl_3$ in eutectic NaCl-UCl_3 molten salt, we found that the reaction $UCl_3 + CrCl_3 = UCl_4 + CrCl_2$ occurs spontaneously, indicating the oxidation of UCl_3 by $CrCl_3$. This reaction was consistently observed in all the NaCl-UCl_3-$CrCl_3$ systems we simulated. As a result, it becomes evident that $CrCl_3$ is not stable in the binary NaCl-UCl_3 mixture.

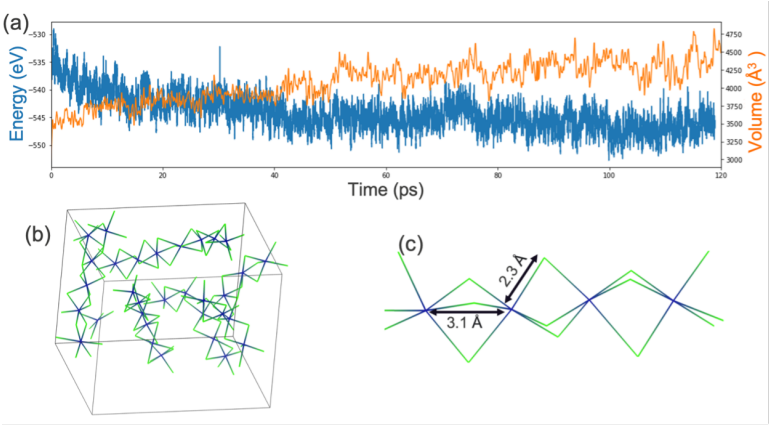

Figure 2.5. (a) Energy and volume evolution of pure $CrCl_3$ at 1100 K from AIMD simulations, (b) snapshot of AIMD trajectories, (c) chain structure in $CrCl_3$.

2.2.4 Pure CsCl and CsCl in eutectic NaCl-UCl_3

Figure 2.6 presents the structure and properties of pure CsCl molten salt from our AIMD simulations. At 1000 K, the simulated density of CsCl is 2.55 g/cm^3, and it decreases to 2.38 g/cm^3 at 1200 K, as indicated in Figure 2.6(b). The simulated density is approximately 5% lower than the experimental data [28]. Regarding the coordination numbers of Cs in CsCl, our simulations reveal that 5-fold and 6-fold coordinated Cs ions are dominant, each comprising approximately 35% of the system. Coordination numbers of 4 and 7 are occurring at approximately 10%. The Cs-Cl bond distance is approximately 3.3 Å, as evidenced by the first peak of the Cs-Cl radial distribution function (RDF) shown in Figure 2.6(c). Notably, the RDFs of CsCl obtained from our simulations exhibit good agreement with experimental data, as depicted by the dashed lines in Figure 2.6(c). This agreement demonstrates the reliability of our simulated results, despite the slight difference in density compared to the experimental measurements. The calculated heat capacity of pure CsCl molten salt is 86 J/mol/K.

In Figure 2.7(a), we present the total energy of the NaCl-UCl_3-CsCl mixture as a function of temperature. It is evident that the total energy also exhibits a linear dependence on temperature. The calculated heat capacity of NaCl-UCl_3-CsCl shows no significant changes with respect to the fraction of CsCl up to 13.5%.

Moving to Figure 2.7(b), we depict the mixing energies resulting from the addition of CsCl in eutectic NaCl-UCl_3. A positive mixing energy is observed for a 3% fraction of CsCl, after which the mixing energy gradually decreases. At a CsCl fraction of 13.5%, the mixing energy reaches -0.02 eV/atom, indicating that CsCl can thermodynamically dissolve in the NaCl-UCl_3 mixture. Furthermore, the calculated mixing energy exhibits insensitivity to temperature variations, demonstrated by the overlapping of mixing energies under different temperature conditions.

Figure 2.7(c) illustrates the calculated densities of NaCl-UCl_3-CsCl from AIMD simulations. Across all systems, the densities decrease linearly with temperature. Upon adding CsCl, the density of the systems shows a slight decrease compared to eutectic NaCl-UCl_3. Additionally, we observe a negative density deviation for all the mixtures as seen in Figure 2.7(d). The magnitude of the density deviation remains within 2% for CsCl fractions up to 13.5%. This negative density deviation suggests that the structures of NaCl-UCl_3-CsCl mixtures are less compact compared to eutectic NaCl-

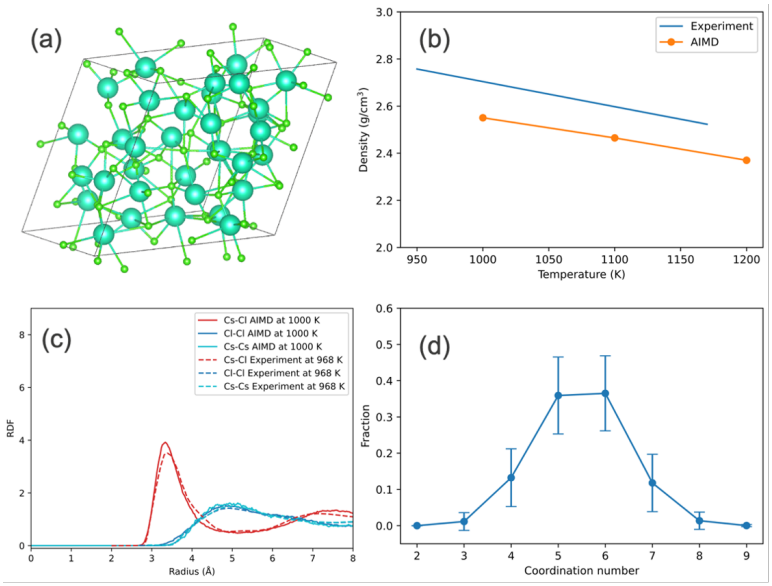

Figure 2.6. Pure CsCl molten salt. (a) Snapshot of AIMD trajectories at 1100 K, (b) density at different temperatures, (c) RDF, and (d) Cr coordination number. The error bars show the standard deviation of density or the fraction of coordination number.

UCl_3 and pure CsCl molten salts. Since pure CsCl molen salt has a heat capacity close to eutectic NaCl-UCl_3, the heat capacity of the NaCl-UCl_3-CsCl mixture is very close to that of eutectic NaCl-UCl_3 as seen in Figure 2.8.

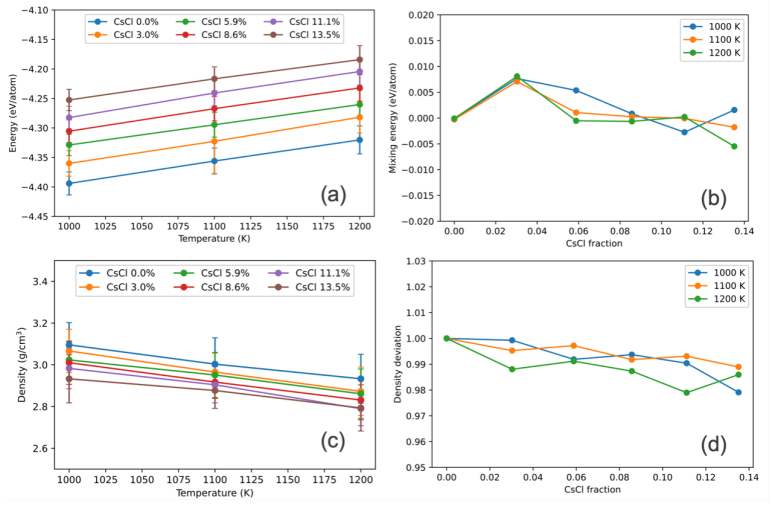

Figure 2.7. (a) Total energy as a function of temperature, (b) mixing energy, (c) density, and (d) density deviation of NaCl-UCl_3-CsCl mixtures.

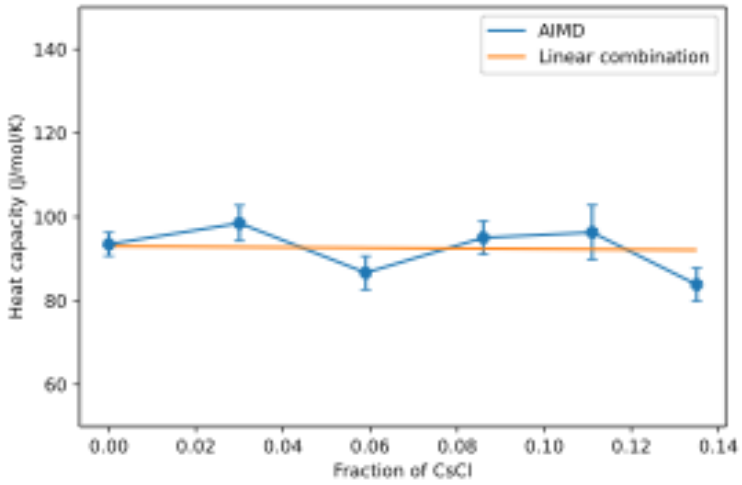

Figure 2.8. Calculated heat capacity of NaCl-UCl_3-CsCl mixtures. The blue lines are calculated from slope of total energy of NaCl-UCl_3-CsCl. The orange line is estimated using a linear combination of the heat capacity of NaCl-UCl_3 and pure CsCl. The error bars are estimated from the slopes of energy in temperature range of 1000 to 1100K, and 1100 to 1200 K.

3. PREDICTION OF THE EFFECTS OF LITHIUM CHLORIDE ON THE THERMOPHYSICAL PROPERTIES OF MNK EUTECTIC SALTS

The second goal of this project in FY23 is to use classical MD simulations to predict the effects of LiCl additive on the thermophysical properties of MNK molten salts. To this end, an ab initio informed empirical potential for describing the $MgCl_2$-NaCl-KCl-LiCl salt system was developed in this work using the force-matching method. To take into account the effects of polarization on molten salt properties, the shell-model potential [32] was employed to model the polarization of the electron cloud of chlorine ions by neighboring cations. Using this empirical potential, we performed classical MD simulations to generate density, heat capacity, enthalpy of mixing, and viscosity data over wide temperature and composition ranges. Our MD simulations showed that, while the addition of LiCl to MNK eutectic salts has little effect on their densities and viscosities, it can significantly increase their specific heat capacities. The modeling methodology and results are summarized in this chapter.

3.1 Computational methodology

3.1.1 Development of shell-model potential for $MgCl_2$-NaCl-KCl-LiCl molten salt system

Since the electronegativity value of Cl (3.16) is much larger than those of Na (0.93), K (0.82), and Li (0.98), the chemical bonding in NaCl, KCl, and LiCl is predominantly ionic. In comparison, the chemical bonding between Mg and Cl is more complex. According to Fajans' rules [33], the degree of anion polarization will be more significant for cations with small sizes and high charges. In addition to having higher charge, the ionic radius of divalent Mg ions (0.72 Å) is smaller than those of monovalent Na (1.02 Å), K (1.38 Å), and Li (0.76 Å) ions. Consequently, while the electronegativity value of Cl is still larger than that of Mg (1.31), the polarization effects can be non-negligible in $MgCl_2$ salt due to the presence of small divalent Mg cations that can strongly polarize the electron cloud surrounding the Cl anions, resulting in partial covalent bonding character.

In this study, the polarizability of monovalent Cl ions is described by the shell model [32]. Here, a Cl ion is separated into a core and a shell, which are linked by a harmonic spring with constant k_{cs}. The total charge of the Cl ion is then the sum of the core charge and shell charge (denoted as Y). The interactions between ions i and j are

described using a Coulomb-Buckingham [34] potential as follows:

$$E_{ij}(r) = q_i q_j \frac{e^2}{r} + A_{ij} e^{-\frac{r}{\rho_{ij}}} - \frac{C_{ij}}{r^6} \tag{3.1}$$

where q_i is the charge of ion i. The first, second, and third term on the right-hand side of the equation represent long-range Coulomb interaction, short-range repulsion, and long-range dispersive interaction, respectively. It is important to note that the Coulomb interaction between a core and its corresponding shell is disregarded in the potential. The values for C_{ij} were calculated in this work using the method of Grimme [35]. The remaining unknown parameters A_{ij}, ρ_{ij}, k_{cs}, and Y were fitted to ab initio forces in structures taken from snapshots of long-time AIMD simulations of pure $MgCl_2$, NaCl, KCl, and LiCl molten salts. Our AIMD simulations employed the generalized gradient approximation of Perdew-Burke-Ernzerhof (PBE) [15] as implemented in the Vienna ab initio simulation package (VASP) [12]. Since local and semi-local density functionals such as PBE cannot describe van der Waals dispersion interactions, which is due to dynamical correlations between fluctuating charge distributions, we employed the density-dependent energy correction (dDsC) method [22] for dispersion correction. We simulated liquid NaCl, KCl, and LiCl using 216-atom supercells, and liquid $MgCl_2$ using 225-atom supercells, all with periodic boundary conditions. A large plane-wave cutoff energy of 500 eV was used to ensure high numerical accuracy. Due to the non-periodicity of the liquid state, a single Γ k-point is sufficient for Brillouin zone sampling.

The final optimized parameters for MNK+LiCl salts are reported in Table 3.1. The partial charge of the Cl ion was set at -0.89. This value was mostly based on our bader charge analysis [36], although it was fine-tuned to achieve the best agreement with ab initio force data. For example, in LiCl, NaCl, and KCl compounds with a rocksalt crystal structure, the partial atomic charges of Cl were calculated to be -0.89, -0.87, and -0.81, respectively. The fixed charges assigned to the cations can be calculated accordingly to ensure charge neutrality. As shown in Figure 3.1, our shell model predicts interatomic forces in pure molten salts in excellent agreement with ab initio values. By assigning an infinite value to k_{cs} to prevent polarization, the resulting rigid-ion potential is still capable of accurately reproducing ab initio forces for NaCl and KCl. However, such a rigid-ion potential gives large errors for $MgCl_2$ and LiCl (see Figure 3.1). It is worth noting that the discovery of non-negligible polarization in LiCl is unexpected, which may be attributed to the significantly smaller size of Li ions compared to Na and K ions.

Table 3.1. Shell-model parameters for $MgCl_2$-NaCl-KCl-LiCl. The optimized values for k_{cs} and Y are 32.735 eV/Å^2 and -3.258, respectively.

i-j	A_{ij} (eV)	ρ_{ij} (Å)	C_{ij} (eVÅ^6)
Cl_s-Cl_s	3068.80	0.3304	52.55 [35]
Mg-Cl_s	2898.08	0.2880	55.77 [35]
Na-Cl_s	3059.82	0.2886	55.77 [35]
K-Cl_s	4086.39	0.3079	76.69 [35]
Li-Cl_s	1970.11	0.2692	29.61 [35]

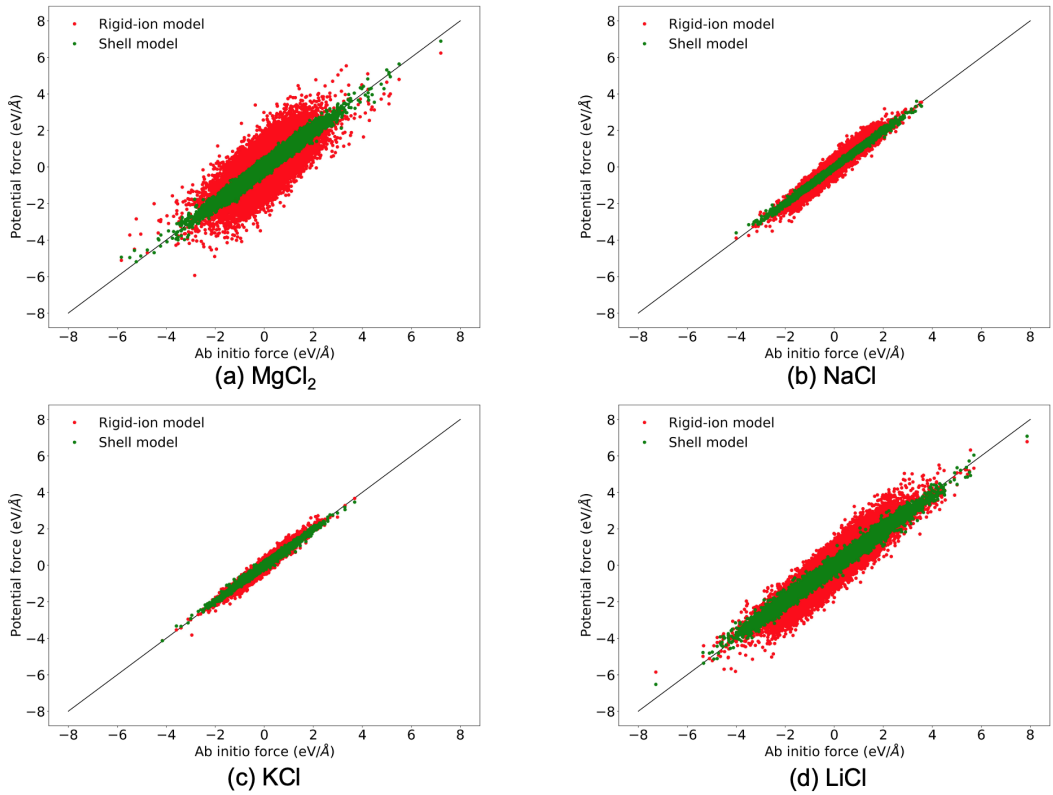

Figure 3.1. Interatomic forces predicted by shell-model and rigid-ion potentials in comparison with ab initio values.

3.1.2 Classical MD simulations

Using our developed empirical potential, we performed classical MD simulations in the Large-scale Atomic/Molecular Massively Parallel Simulator (LAMMPS) [37] to predict the thermophysical properties of pure chloride salts and their binary/ternary mixtures in the $MgCl_2$-NaCl-KCl-LiCl system over wide temperature and composition ranges. The Newton's equations of motion were numerically solved using Verlet's algorithm with a time step of 0.5 femtosecond. For obtaining equilibrium densities, heat capacities, and viscosities, periodic cubic simulation cells containing over 10,000 atoms were employed. At a given temperature, MD simulations in the NPT (constant number of atoms, pressure, and temperature) ensemble were first performed to obtain the equilibrium lattice parameter. Subsequently, long-time MD trajectories exceeding 1 nanosecond in the NVT (constant number of atoms, volume, and temperature) ensemble were collected to extract viscosity data.

The constant pressure heat capacity of a molten salt is defined as the first derivative of its enthalpy with respect to temperature:

$$C_p = \frac{dH}{dT} \tag{3.2}$$

In this study, this derivative is numerically evaluated through linear fitting of MD-calculated enthalpy vs. temperature

data over a wide temperature range. For simplicity, the temperature dependence of C_p is neglected. The specific heat capacity can be determined by dividing C_p by the molar mass of the salt.

Using the Green-Kubo relation, viscosity can be obtained from equilibrium MD simulations via time integral of the off-diagonal terms of the stress autocorrelation function as:

$$\eta = \frac{V}{k_B T} \int_0^\infty \langle p_{xy}(0) p_{xy}(t) \rangle dt \tag{3.3}$$

where V is volume, p_{xy} is the off-diagonal component of the stress tensor, and k_B is the Boltzmann constant.

According to the Einstein relation, the self-diffusivities of ions can be determined from their time-dependent mean squared displacement (MSD) data as:

$$D = \lim_{t \to \infty} \frac{MSD}{6t} \tag{3.4}$$

where the MSD of atoms of type i and can be calculated as:

$$MSD = \frac{1}{N_i} \sum_{j=1}^{N_i} |R_j(t) - R_j(0)|^2 \tag{3.5}$$

3.2 Results and discussion

3.2.1 Thermophysical properties of pure salts

For validation purposes, we first calculated the densities, specific heat capacities, and viscosities of pure molten salts using our developed shell-model potential, and the results are compared with existing experimental data [38, 39, 40, 41, 42, 43, 44] in Figures 3.2, 3.3, and 3.4, respectively. Overall, the shell-model potential predicts heat capacities and viscosities in reasonable agreement with experimental measurements. For densities, however, there exist larger discrepancies. As shown in Figure 3.2, the shell-model potential overestimates the densities of liquid $MgCl_2$ by around 10% and underestimates the densities of liquid KCl by around 12% at their respective melting points. Due to the very low bulk moduli of molten salts, their MD-predicted equilibrium densities can be highly sensitive to the empirical potential used. As has been recently demonstrated by Faheem and Lee [45], further improvement to our shell-model potential can be made in future studies by explicitly including thermophysical properties such as density in the fitness function during parameter optimization.

3.2.2 Thermodynamic and thermophysical properties of binary salt mixtures

Figure 3.5 shows the MD-calculated enthalpies of mixing for NaCl-KCl, NaCl-LiCl, KCl-LiCl, $MgCl_2$-KCl, $MgCl_2$-NaCl, and $MgCl_2$-LiCl molten salt mixtures in overall good agreement with available experimental data [46], AIMD simulations [47, 48], and CALPHAD (CALculation of PHAse Diagrams) modeling [49]. Although mixing enthalpy data were not used in the potential fitting process, our shell-model potential correctly predicts that $MgCl_2$-KCl salts exhibit significantly more negative enthalpies of mixing than those of $MgCl_2$-NaCl and $MgCl_2$-LiCl salts. Furthermore,

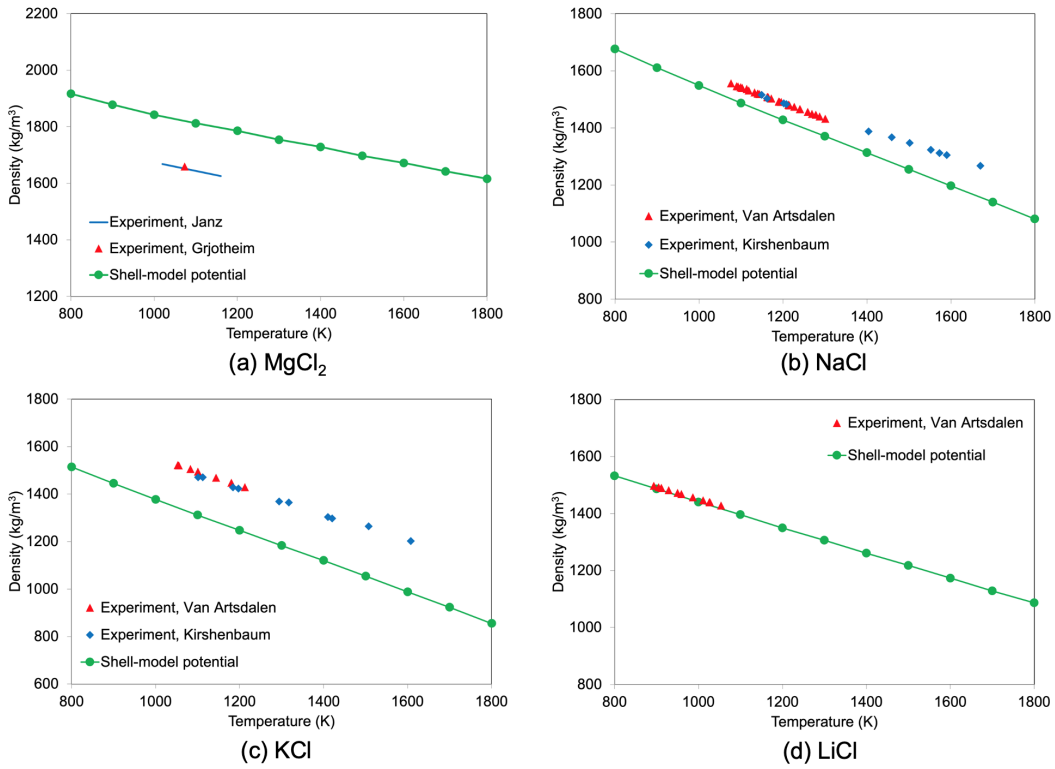

Figure 3.2. MD-predicted densities of pure molten salts in comparisons with experimental measurements from Janz et al. [38], Grjotheim et al. [39], Van Artsdalen and Yaffe [40], and Kirshenbaum et al. [41].

consistent with AIMD simulations [47] and CALPHAD modeling [49], our shell-model potential predicts ideal mixing behavior in NaCl-KCl system. Such good agreement suggests that the potential developed in this study can also predict thermodynamic properties with reasonable accuracy.

Figures 3.6, 3.7, and 3.8 further show the MD-calculated densities, specific heat capacities, and viscosities of binary salt mixtures in the $MgCl_2$-NaCl-KCl-LiCl system. With the exceptions of the densities of KCl-rich and $MgCl_2$-rich salt mixtures, overall good agreement has been observed between modeling and experiments [38, 39, 48, 50, 51, 52, 53]. For the viscosities of $MgCl_2$-KCl salt mixtures, our shell-model potential yields results that agree reasonably well with the experimental data from Janz [50]. However, it notably underestimates viscosity compared to the experimental data from Xu et al. [52]. Resolving this discrepancy may necessitate further experimental measurements. Importantly, adding LiCl to pure NaCl, KCl, and $MgCl_2$ molten salts will significantly increase their specific heat capacities, as shown in Figure 3.7. Furthermore, while the addition of LiCl to MgCl2 will decrease its viscosity, the viscosities of NaCl-LiCl and KCl-LiCl salt mixtures are almost independent of their compositions (see Figure 3.8).

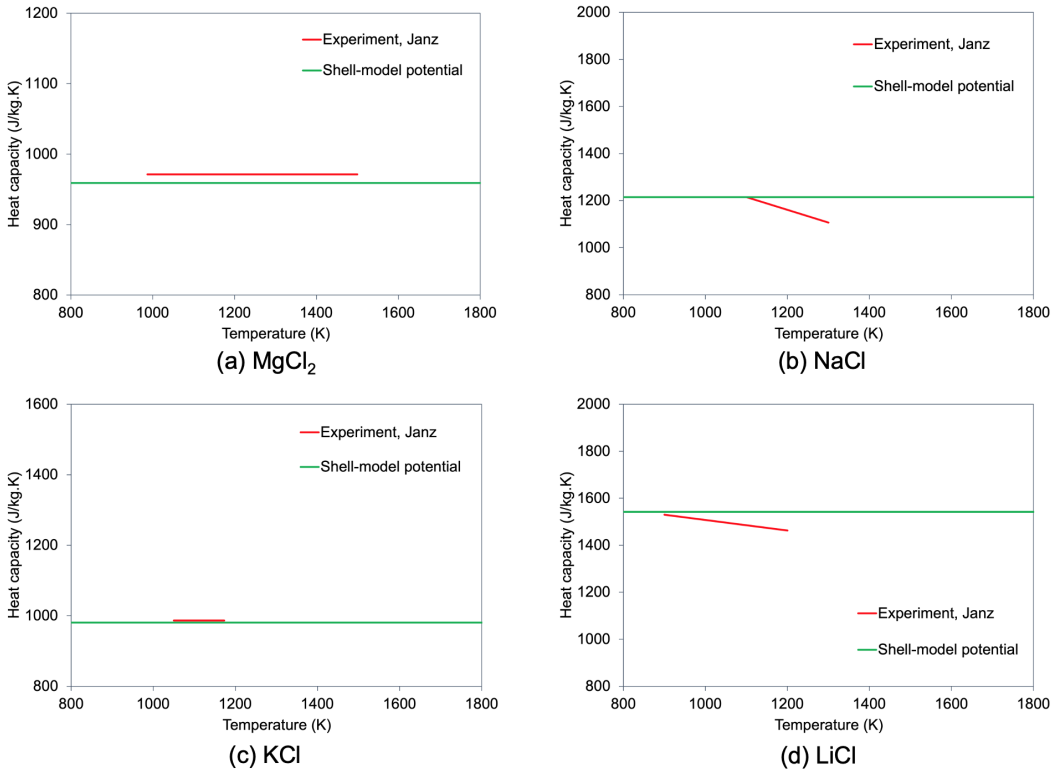

Figure 3.3. MD-predicted specific heat capacities of pure molten salts in comparisons with experimental measurements from Janz et al. [38].

3.2.3 Structures of MNK eutectic salts

Figure 3.9 presents the MD-predicted radial distribution functions (RDFs) for 45$MgCl_2$+33NaCl+22KCl and 38$MgCl_2$+21NaCl+41KCl eutectic salts at a temperature of 750 K. The prominent first peak observed in the Mg-Cl RDF arises from the formation of stable $MgCl_n$ complexes. The positions of the first peaks in the RDFs give the nearest-neighbor Mg-Cl, Na-Cl, K-Cl, Cl-Cl, Mg-Mg, Na-Na, and K-K bond lengths. Remarkably, the first peak positions, as predicted by our shell-model potential, closely match those from AIMD simulations by Li et al. [54]. Figures 3.10a and 3.11a further present the average coordination numbers (CNs) of Cl ions around Mg ions in both eutectic salts. This information can be obtained by integrating over the first peak of the RDF for the Mg-Cl pair. For 45$MgCl_2$+33NaCl+22KCl, our MD-predicted CN values agree well with the AIMD simulations by Li et al. [54]. Both MD and AIMD simulations indicate a reduction in the coordination number of Mg as the temperature increases. Our detailed analysis, as shown in Figure 3.10b, reveals that 5-fold and 4-fold coordinated Mg ions predominate in 45$MgCl_2$+33NaCl+22KCl at temperatures below and above 900 K, respectively. In 38$MgCl_2$+21NaCl+41KCl, the majority of Mg ions prefer a 4-fold coordination by Cl atoms at all temperatures (Figure 3.11b). Our findings for the structures of MNK eutectic salts are fully consistent with the Raman study by Brooker [55], which provided direct evidence for the predominance of $MgCl_4$ tetrahedrons in K2MgCl4 molten salt.

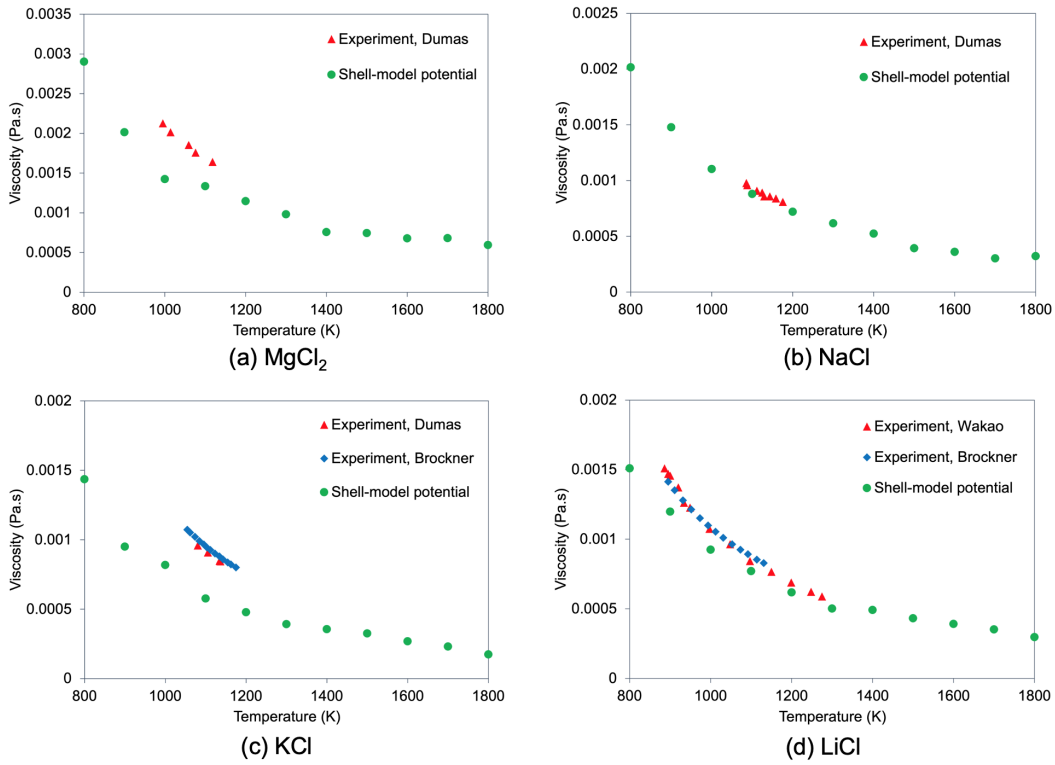

Figure 3.4. MD-predicted viscosities of pure molten salts in comparisons with experimental measurements from Dumas et al. [42], Brockner et al. [43], and Wakao et al. [44].

The MD snapshots for both MNK salts are depicted in Figures 3.10d and 3.11d. It can be observed that $MgCl_n$ polyhedrons form a network structure through corner, edge, or face sharing. Further insight into the distribution of Mg ions among monomers ($MgCl_n$), dimers (Mg_2Cl_n), trimers (Mg_3Cl_n), and larger oligomers (Mg_mCl_n with m>3) is shown in Figures 3.10c and 3.11c. While over 80% of $MgCl_n$ polyhedrons in $45MgCl_2$+33NaCl+22KCl are interconnected to form oligomers comprising more than three Mg ions, this fraction decreases to around 60% in $38MgCl_2$+21NaCl+41KCl due to its reduced $MgCl_2$ concentration. Note that, at high temperatures, larger oligomers tend to dissociate, leading to increased concentrations of Mg monomers, dimers, or trimers.

3.2.4 Thermophysical properties of MNK eutectic salts and the effects of LiCl

Figures 3.12 and 3.13 show the thermophysical properties and ionic self-diffusivities for the eutectic salt compositions $45MgCl_2$+33NaCl+22KCl and $38MgCl_2$+21NaCl+41KCl as predicted by our MD simulations with the shell-model potential. For both densities and heat capacities, our results demonstrate good agreement with both experimental data [54, 6] and AIMD simulations [54]. Remarkably, the order of ionic self-diffusion coefficients predicted by our MD simulations, $D_{Na}>D_K>D_{Cl}>D_{Mg}$, is fully consistent with Li et al.'s AIMD simulations [54]. For both eutectic salts, the viscosities determined using the Green-Kubo method are in excellent agreement with the values predicted by the

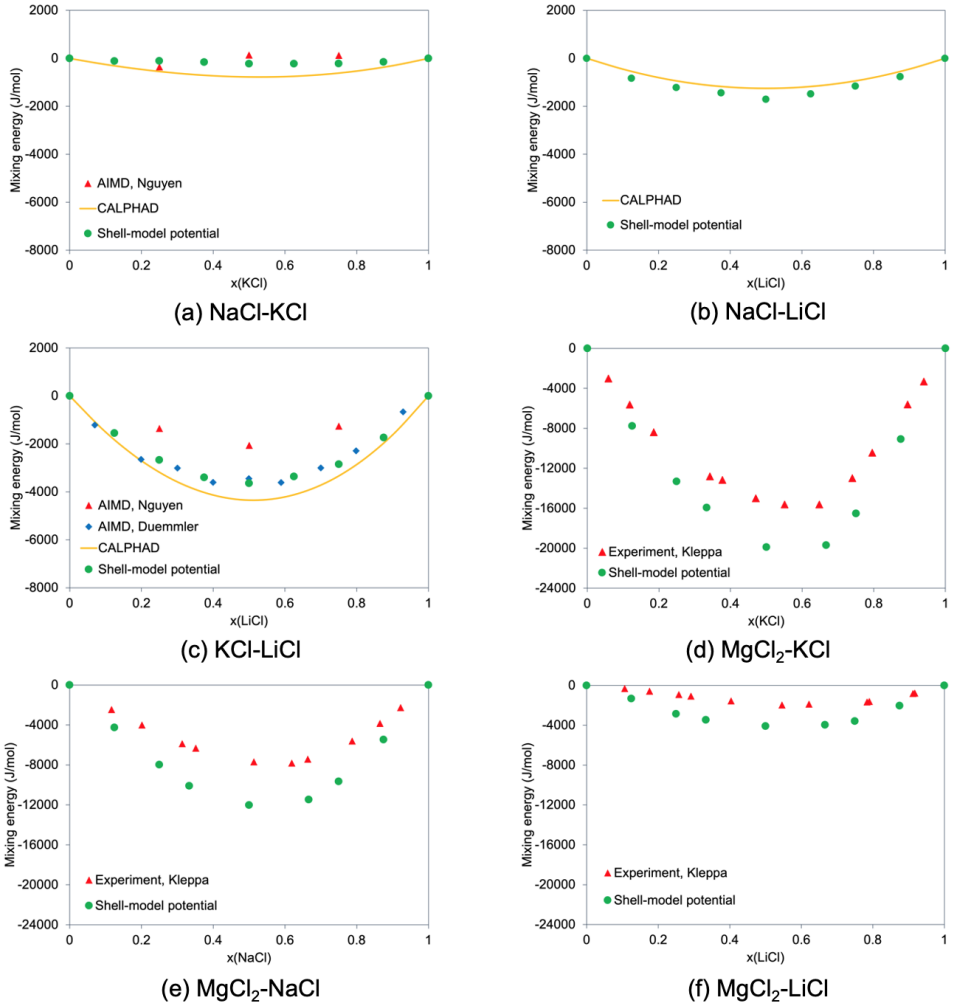

Figure 3.5. MD-predicted mixing enthalpies of binary molten salt mixtures in comparisons with experimental measurements from Kleppa and McCarty [46], AIMD simulations by Nguyen et al. [47] and Duemmler et al. [48], and CALPHAD modeling by Hao et al. [49].

Stokes-Einstein relation [47, 54]:

$$\eta = \frac{k_B T}{2\pi D d} \tag{3.6}$$

where D represents the composition-weighted average of the self-diffusion coefficients for Mg, Na, K, and Cl, which have been calculated in our MD simulations (see Figures 3.12(d) and 3.13(d)) and in the AIMD simulations by Li et al. [54]. The hydrodynamic radius d can be calculated using the nearest-neighbor bond distances obtained from the RDF plots in Figure 3.9 as:

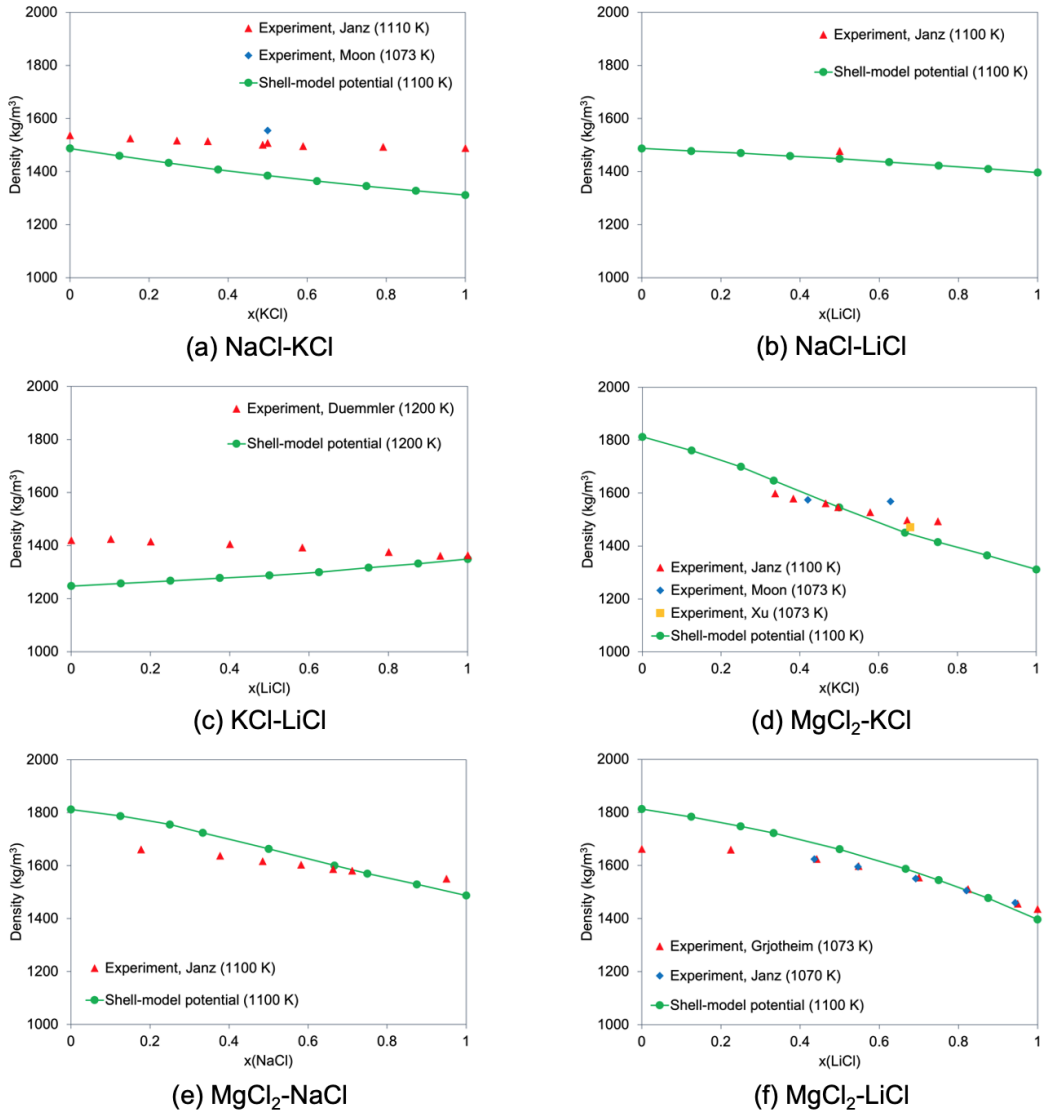

Figure 3.6. MD-predicted densities of binary molten salt mixtures in comparisons with experimental measurements from Janz et al. [38, 50], Moon et al. [51], Duemmler et al. [48], Xu et al. [52], and Grjotheim et al. [39].

$$d = \frac{d_{Mg-Mg} + d_{Na-Na} + d_{K-K} + d_{Cl-Cl} + 2d_{Mg-Cl} + 2d_{Na-Cl} + 2d_{K-Cl}}{10} \tag{3.7}$$

While our shell-model potential predicts viscosities for 45$MgCl_2$+33NaCl+22KCl that align with the AIMD study by Li et al. [54] (see Figure 3.12(c)), it underestimates viscosity for 38$MgCl_2$+21NaCl+41KCl compared to the experimental data from Wang et al. [6] (see Figure 3.13(c)). Future experimental studies will be needed to bridge this disparity.

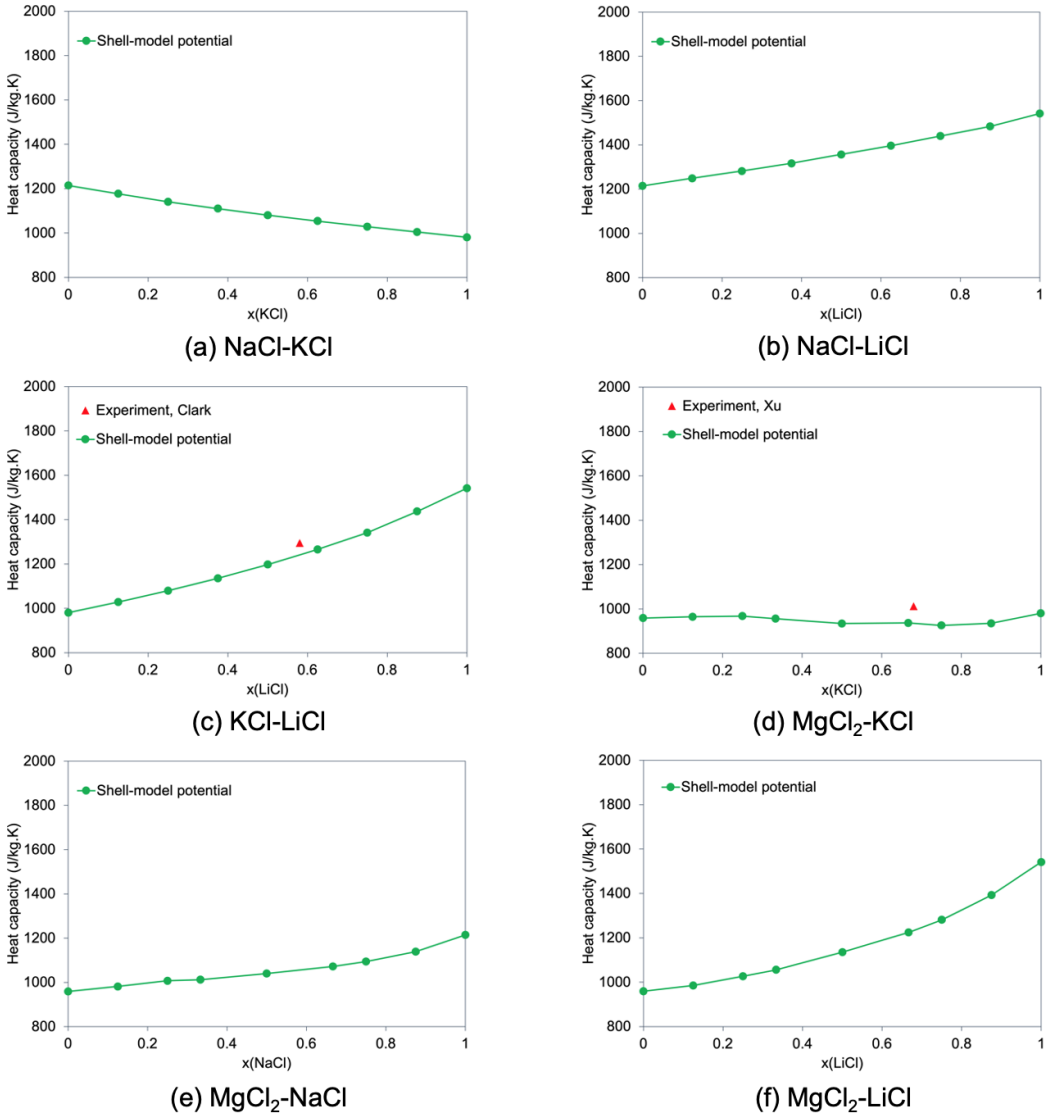

Figure 3.7. MD-predicted specific heat capacities of binary molten salt mixtures in comparisons with experimental measurements from Clark [53] and Xu et al. [52].

Finally, Figures 3.14 and 3.15 illustrate the effects of LiCl addition on the thermophysical characteristics of MNK eutectic salts, as predicted by the present MD simulations. The incorporation of LiCl into MNK salts minimally changes their densities and viscosities. However, it significantly increases their specific heat capacities, which is beneficial for high-temperature heat transfer applications. For example, adding 10% (20%) of LiCl to 45$MgCl_2$+33NaCl+22KCl and 38$MgCl_2$+21NaCl+41KCl results in an increase of 3.4% (6.1%) and 3.8% (8.9%) in specific heat capacity, respectively. In future studies, our shell-model potential can be harnessed to guide the search for molten salt compositions within the $MgCl_2$-NaCl-KCl-LiCl quaternary system that strike the optimal balance between performance and cost [56].

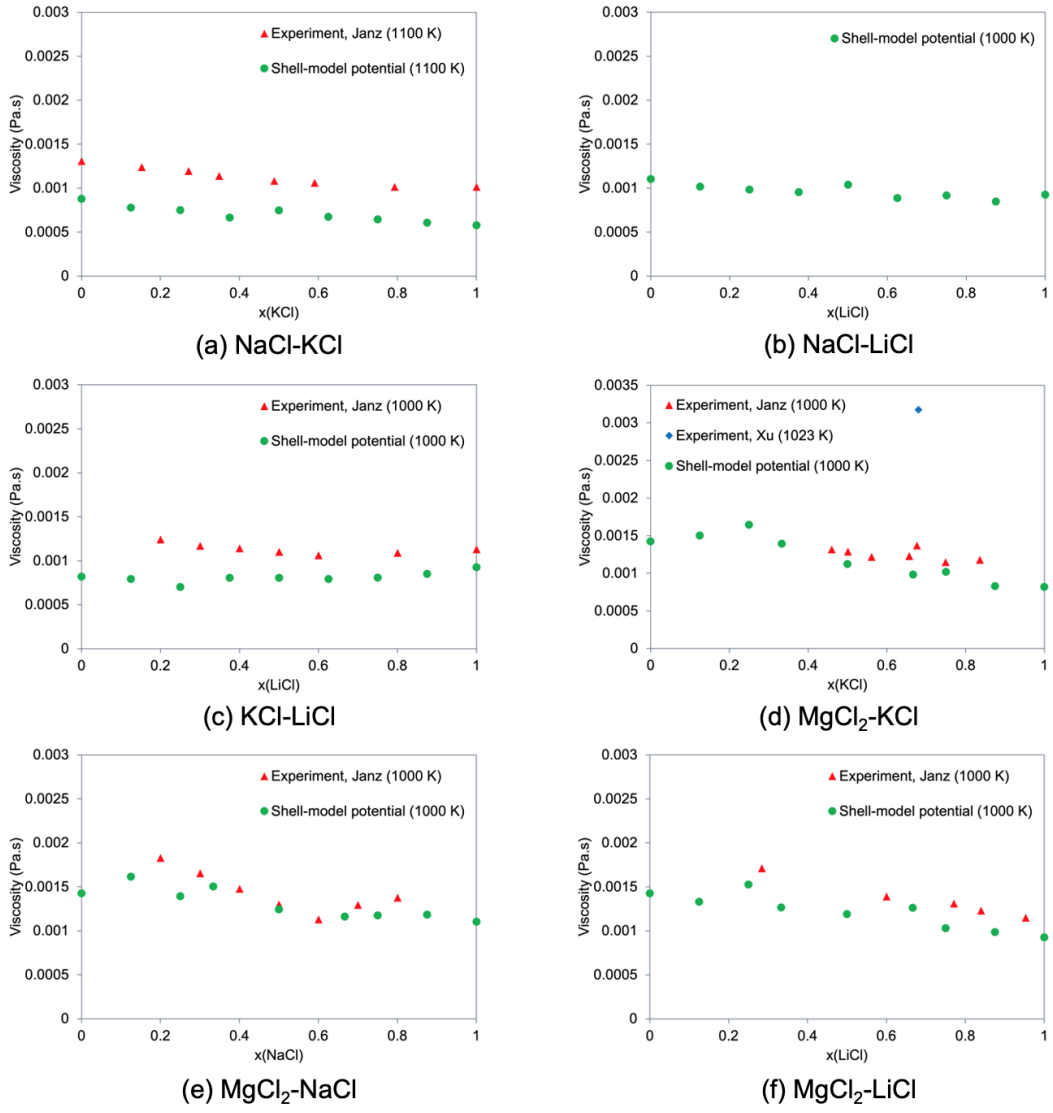

Figure 3.8. MD-predicted viscosities of binary molten salt mixtures in comparisons with experimental measurements from Janz et al. [38, 50] and Xu et al. [52].

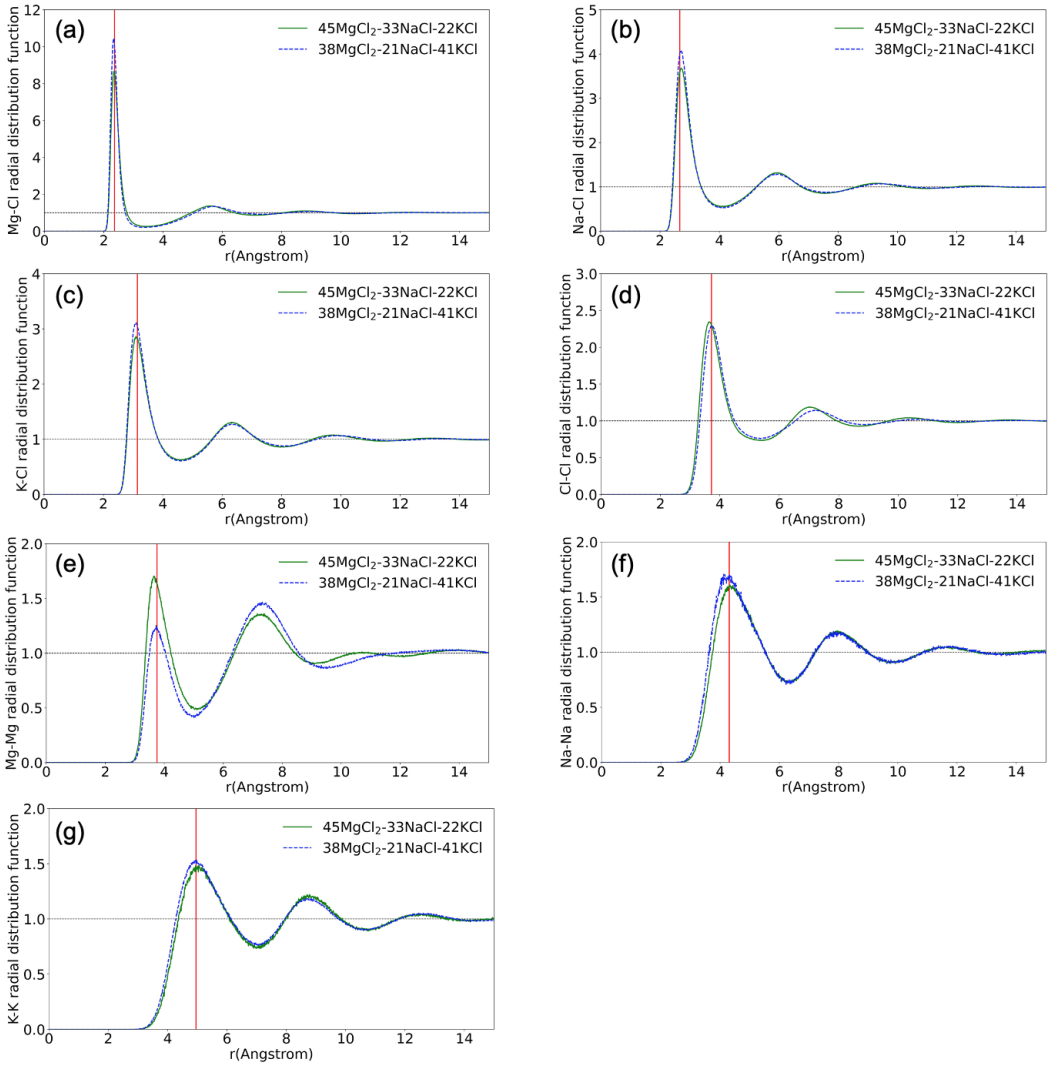

Figure 3.9. MD-predicted radial distribution functions of (a) Mg-Cl, (b) Na-Cl, (c) K-Cl, (d) Cl-Cl, (e) Mg-Mg, (f) Na-Na, and (g) K-K pairs in $45MgCl_2$+33NaCl+22KCl and $38MgCl_2$+21NaCl+41KCl eutectic mixtures at 750 K. The vertical red lines indicate the first peak positions from AIMD simulations at 723 K by Li et al. [54].

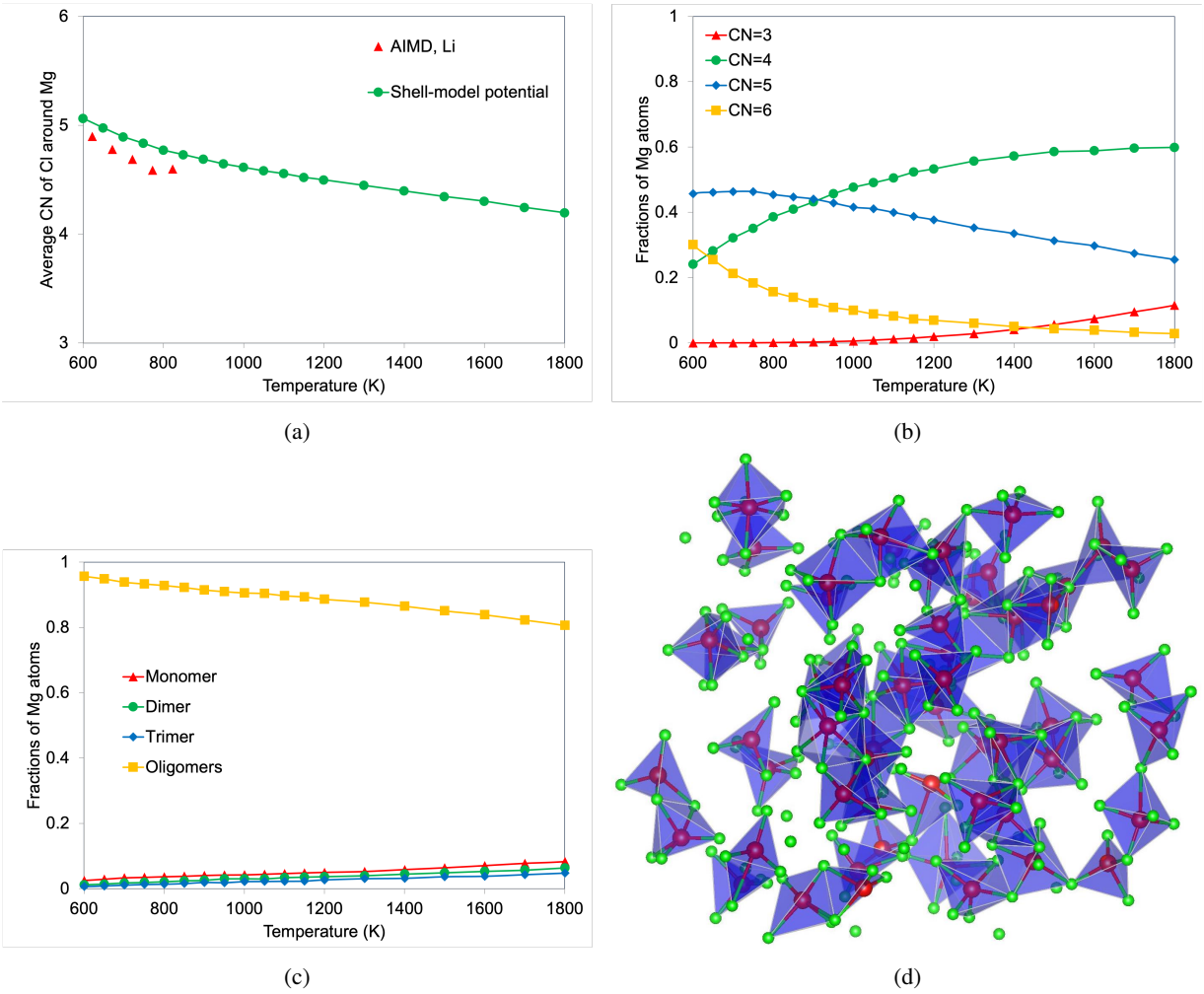

Figure 3.10. (a) MD-predicted average coordination numbers of Cl around Mg in $45MgCl_2$+33NaCl+22KCl salt in comparison with AIMD simulations by Li et al. [54]. (b) Fractions of three-fold, four-fold, five-fold, and six-fold coordinated Mg atoms. (c) Fractions of Mg atoms in monomers, dimers, trimers, and larger oligomers. (d) A snapshot of $45MgCl_2$+33NaCl+22KCl salt at 750 K. Red and green spheres represent Mg and Cl atoms, respectively. For visualization of the Mg network, Na and K atoms are not shown.

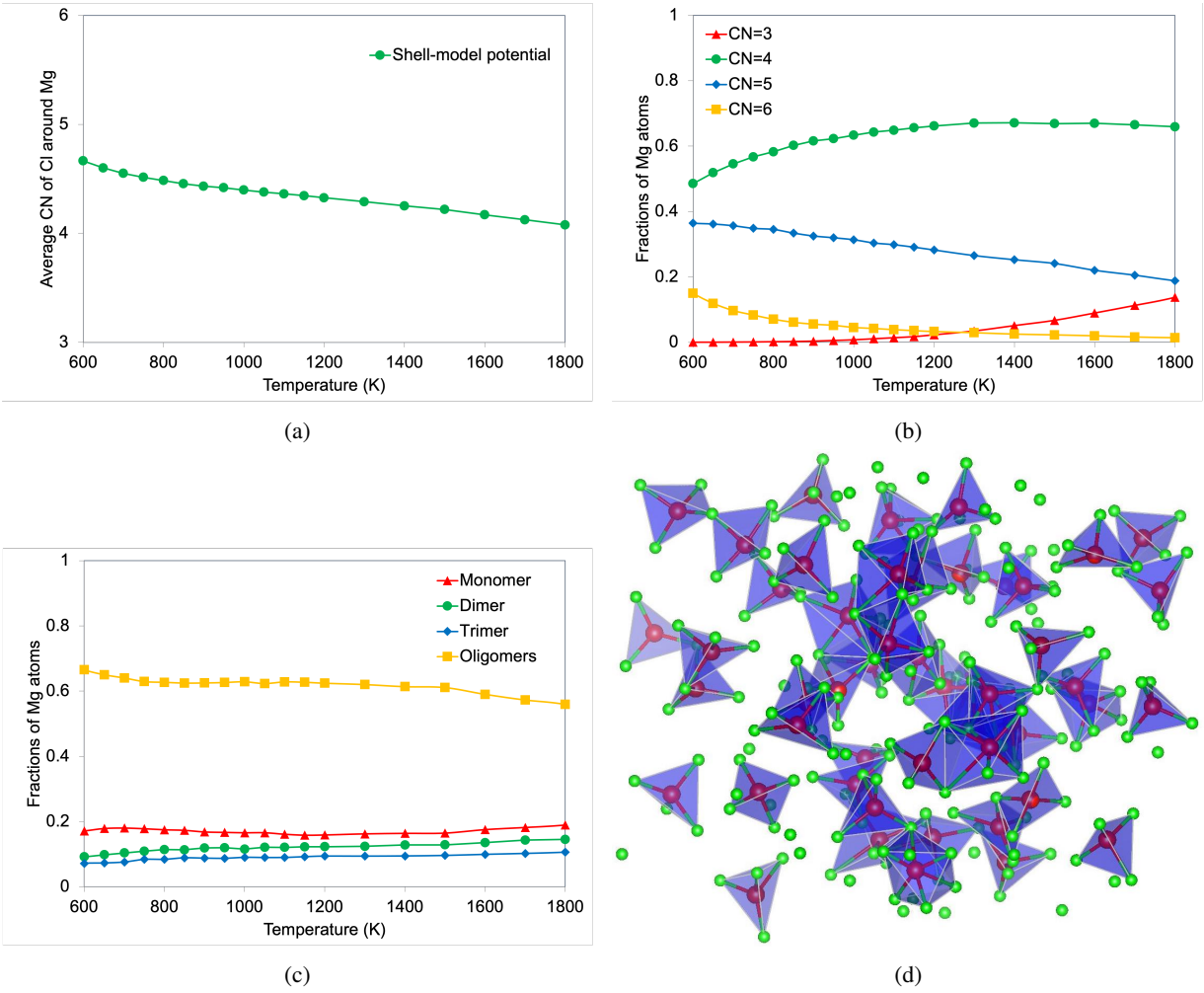

Figure 3.11. (a) MD-predicted average coordination numbers of Cl around Mg in $38MgCl_2$+21NaCl+41KCl salt. (b) Fractions of three-fold, four-fold, five-fold, and six-fold coordinated Mg atoms. (c) Fractions of Mg atoms in monomers, dimers, trimers, and larger oligomers. (d) A snapshot of $38MgCl_2$+21NaCl+43KCl salt at 750 K. Red and green spheres represent Mg and Cl atoms, respectively. For visualization of the Mg network, Na and K atoms are not shown.

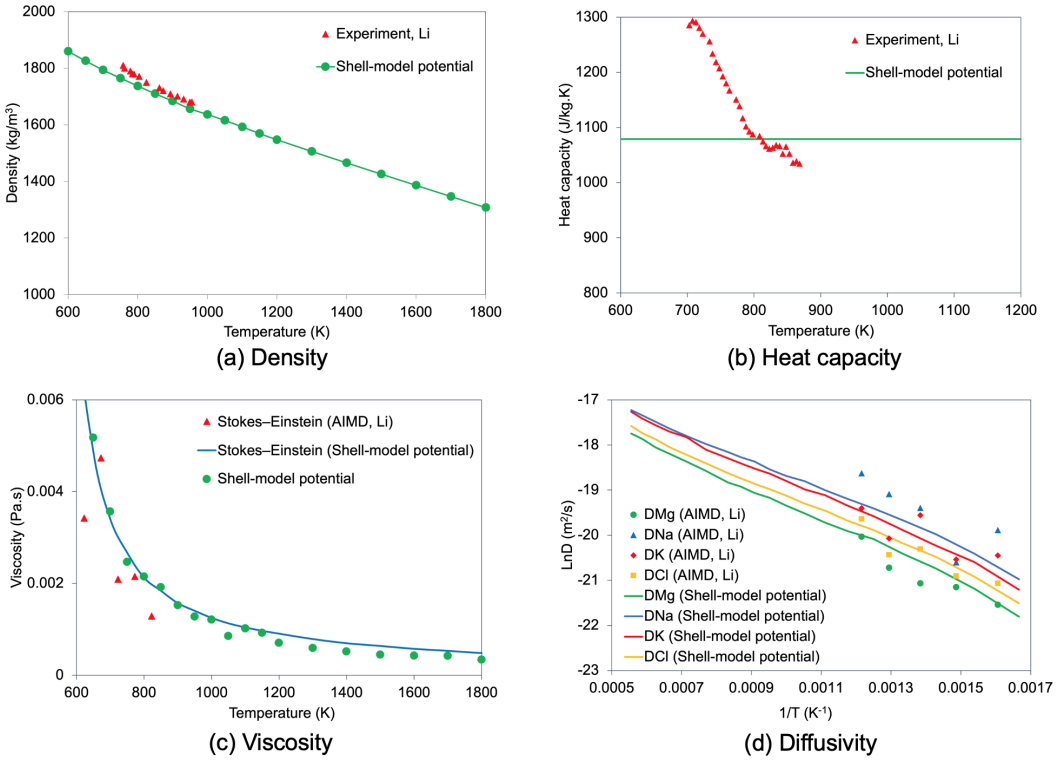

Figure 3.12. MD-predicted thermophysical properties for $45MgCl_2$+33NaCl+22KCl salt in comparisons with experimental measurements and AIMD simulations by Li et al. [54]. Ionic self-diffusivities from our MD simulations and from AIMD simulations by Li et al. [54] are shown in (d).

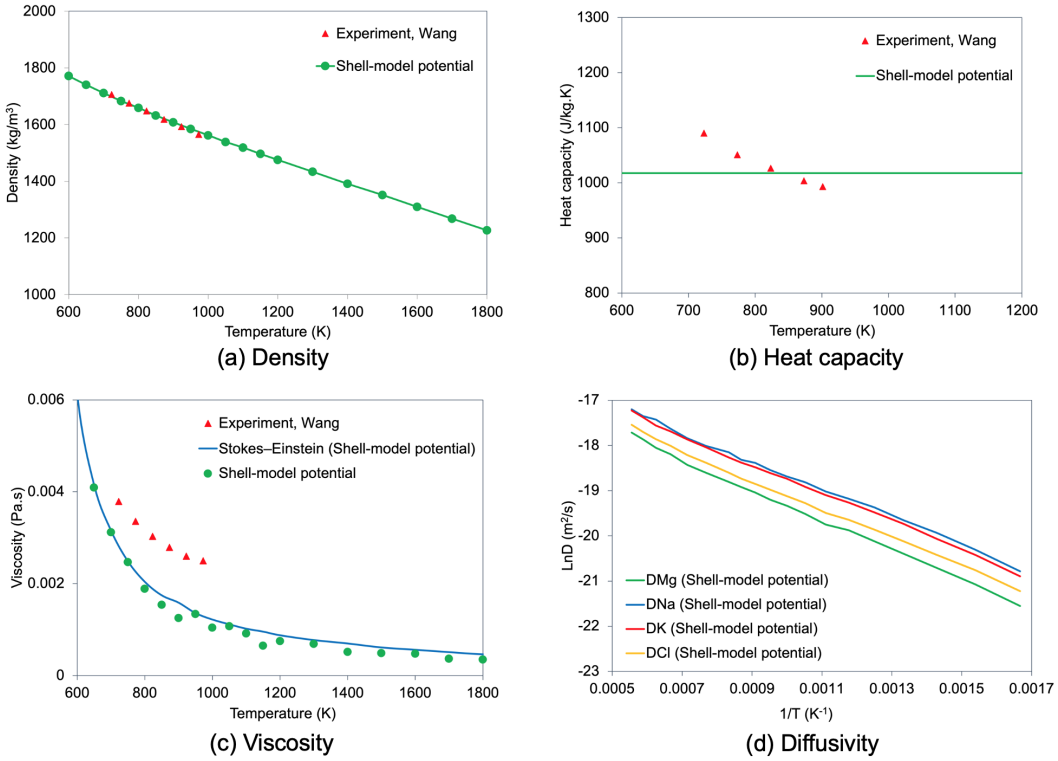

Figure 3.13. MD-predicted thermophysical properties for $38MgCl_2$+21NaCl+41KCl salt in comparisons with experimental measurements by Wang et al. [6]. Results for ionic self-diffusivities from our MD simulations are shown in (d).

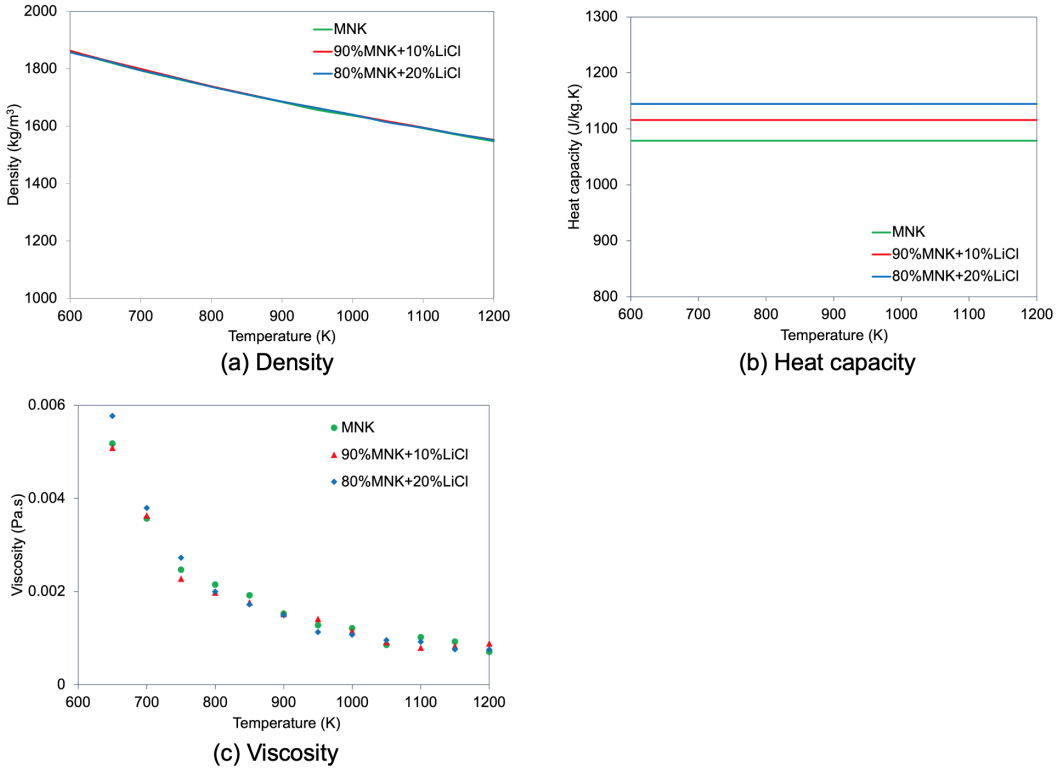

Figure 3.14. The effects of LiCl on the thermophysical properties of $45MgCl_2$+33NaCl+22KCl salt mixture.

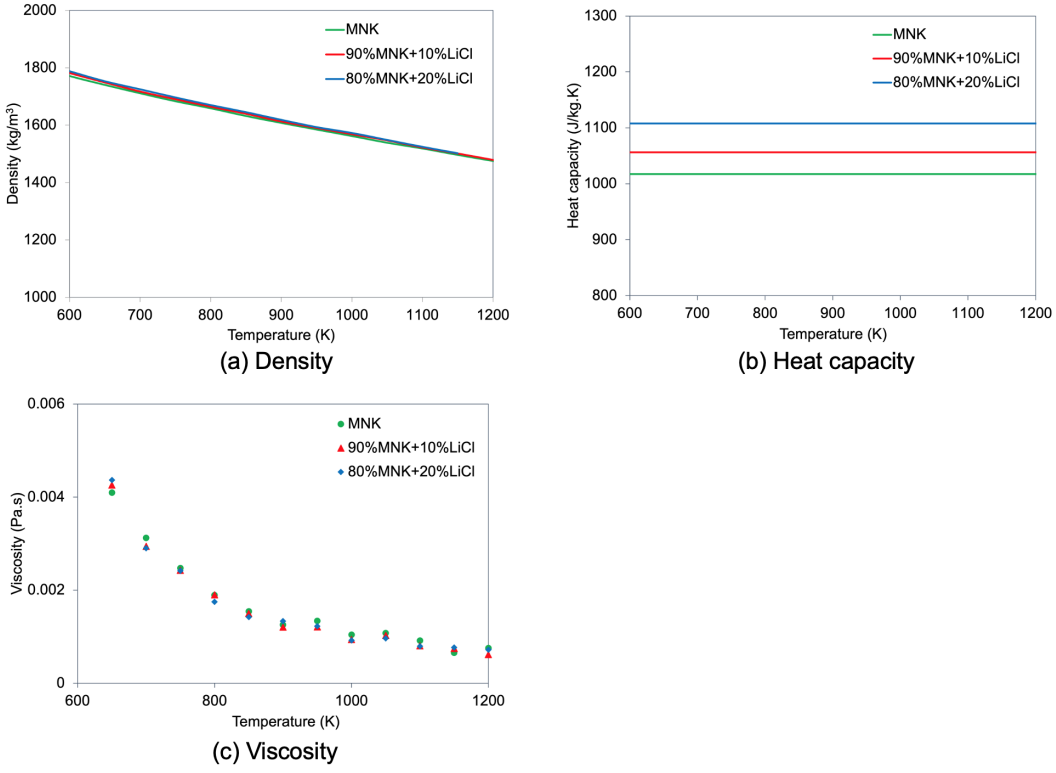

Figure 3.15. The effects of LiCl on the thermophysical properties of $38MgCl_2$+21NaCl+41KCl salt mixture.

4. SUMMARY

In this study, AIMD simulations were conducted to explore the structural and thermophysical properties of eutectic NaCl-UCl_3 molten salt with the presence of corrosion products ($CrCl_2$ and $CrCl_3$) and a fission product (CsCl). The molar concentration of these corrosion and fission products had minimal impact on the coordination number and radial distribution function of U. The introduction of $CrCl_2$ and CsCl caused a reduction in the density of the mixtures compared to eutectic NaCl-UCl_3. Notably, $CrCl_2$ exhibited a negative mixing energy in NaCl-UCl_3, and the mixing energy decreased as the $CrCl_2$ molar concentration increased. On the other hand, a positive mixing energy was observed for a 3% fraction of CsCl, which gradually decreased -0.02 eV/atom at a CsCl fraction of 13.5%. The negative mixing energy of $CrCl_2$ and CsCl indicates the thermodynamic dissolution of $CrCl_2$ and CsCl in the NaCl-UCl_3 mixture. Modeling $CrCl_3$ presented significant challenges because of the coordination chemistry of Cr^{3+}. $CrCl_3$ cannot exist in eutectic NaCl-UCl_3 since it would be reduced to $CrCl_2$ by UCl_3.

As the second part of this study, we performed classical MD simulations to predict the densities, specific heat capacities, viscosities, and ionic self-diffusivities for MNK eutectic salts over a wide temperature range. The impact of LiCl additive on their thermophysical properties, as well as the network structure in MNK salts, were further investigated. To capture the electronic polarization of Cl anions by neighboring cations, we developed a shell-model potential using the force-matching method and a dataset of ab initio-calculated interatomic forces. Our extensive MD simulations predicted properties for pure salts, as well as binary and ternary salt mixtures, in the $MgCl_2$-NaCl-KCl-LiCl system in overall good agreement with available experimental and theoretical data in the literature, which corroborated the accuracy and reliability of our developed potential.

Bibliography

[1] G. Locatelli, M. Mancini, and N. Todeschini. “Generation IV nuclear reactors: Current status and future prospects”. In: *Energy Policy* 61 (2013), pp. 1503 –1520.

[2] B. Li, S. Dai, and D. Jiang. “First-principles molecular dynamics simulations of UCl_n–NaCl(n= 3, 4) Molten Salts”. In: *ACS Applied Energy Materials* 2 (2019), pp. 2122 –2128.

[3] W. R. Grimes. “Molten-salt reactor chemistry”. In: *Nuclear Applications and Technology* 8 (1970), pp. 137 – 155.

[4] D. E. Holcomb et al. *Fast spectrum molten salt reactor options*. Tech. rep. ORNL/TM-2011/105. Oak Ridge National Laboratory, 2011.

[5] T. Hartmann and P. D. Paviet. “Corrosion of Containment Alloys in Molten Salt Reactors and the Prospect of Online Monitoring”. In: *Journal of Nuclear Fuel Cycle and Waste Technology* 20 (2022), pp. 43–63.

[6] X. Wang et al. “Thermophysical properties experimentally tested for NaCl-KCl-$MgCl_2$ eutectic molten salt as a next-generation high-temperature heat transfer fluids in concentrated solar power systems”. In: *J. Sol. Energy Eng.* 143 (2021), p. 041005.

[7] C. Villada et al. “Engineering molten $MgCl_2$–KCl–NaCl salt for high-temperature thermal energy storage: Review on salt properties and corrosion control strategies”. In: *Sol. Energy Mater. Sol. Cells* 232 (2021), p. 111344.

[8] B. C. Kelleher, S. F. Gagnon, and I. G. Mitchell. “Thermal gradient mass transport corrosion in NaCl-$MgCl_2$ and $MgCl_2$-NaCl-KCl molten salts”. In: *Materials Today Communications* 33 (2022), p. 104358.

[9] K. Sridharan and T. Allen. “Corrosion in molten salts”. In: *Molten salts chemistry*. Elsevier, 2013, pp. 241–267.

[10] N. Winner et al. “Ab-initio simulation studies of chromium solvation in molten fluoride salts”. In: *Journal of Molecular Liquids* 335 (2021), p. 116351.

[11] C. F. Baes Jr. “The chemistry and thermodynamics of molten salt reactor fuels”. In: *Journal of Nuclear Materials* 51 (1974), pp. 149–162.

[12] G. Kresse and J. Furthmuller. “Efficient iterative schemes for ab initio total-energy calculations using a plane-wave basis set”. In: *Phys. Rev. B* 54 (1996), pp. 11169–11186.

[13] G. Kresse and J. Furthmuller. “Efficiency of ab-initio total energy calculations for metals and semiconductors using a plane-wave basis set”. In: *Computational Materials Science* 6 (1996), pp. 15 –50.

[14] P. E. Blochl. “Projector augmented-wave method”. In: *Phys. Rev. B* 50 (1994), pp. 17953–17979.

[15] J. P. Perdew, K. Burke, and M. Ernzerhof. “Generalized gradient approximation made simple”. In: *Physical Review Letters* 77 (1996), pp. 3865–3868.

[16] A. Rohrbach, J. Hafner, and G. Kresse. “Electronic correlation effects in transition-metal sulfides”. In: *Journal of Physics: Condensed Matter* 15 (2003), p. 979.

[17] B. Himmetoglu et al. “Hubbard-corrected DFT energy functionals: The LDA+U description of correlated systems”. In: *International Journal of Quantum Chemistry* 114 (2014), pp. 14 –49.

[18] S. Dudarev et al. “Electronic structure and elastic properties of strongly correlated metal oxides from first principles: LSDA+U, SIC-LSDA and EELS study of UO_2 and NiO”. In: *Physica Status Solidi (a)* 166 (1998), pp. 429 –443.

[19] S. L. Dudarev et al. “Electron-energy-loss spectra and the structural stability of nickel oxide: An LSDA+U study”. In: *Physical Review B* 57 (1998), p. 1505.

[20] D. Andersson and B. Beeler. “Ab initio molecular dynamics (AIMD) simulations of NaCl, UCl_3 and NaCl-UCl_3 molten salts”. In: *Journal of Nuclear Materials* 568 (2022), p. 153836.

[21] F. Xue et al. “Two-dimensional ferromagnetic van der Waals $CrCl_3$ monolayer with enhanced anisotropy and Curie temperature”. In: *Physical Review B* 100 (2019), p. 224429.

[22] S. N. Steinmann and C. Corminboeuf. “Comprehensive benchmarking of a density-dependent dispersion correction”. In: *J. Chem. Theory Comput.* 7 (2011), pp. 3567 –3577.

[23] S. N. Steinmann and C. Corminboeuf. “A generalized-gradient approximation exchange hole model for dispersion coefficients”. In: *The Journal of Chemical Physics* 134 (2011), p. 044117.

[24] H. Kim, J. M. Choi, and W. A. Goddard III. “Universal correction of density functional theory to include London dispersion (up to Lr, element 103)”. In: *The Journal of Physical Chemistry Letters* 3 (2012), pp. 360–363.

[25] P. Schwerdtfeger and J. K. Nagle. “2018 Table of Static Dipole Polarizabilities of the Neutral Elements in the Periodic Table”. In: *Mol. Phys.* 117 (2019), pp. 1200–1225.

[26] M. P. Allen and D. J. Tildesley. *Computer simulation of liquids*. Oxford university press, 2017.

[27] G. J. Janz et al. “Molten salts: volume 4, Part 1, fluorides and mixtures electrical conductance, density, viscosity, and surface tension data”. In: *Journal of Physical and Chemical Reference Data* 3 (1974), pp. 1–115.

[28] G. J. Janz et al. “Molten salts: volume 4, part 2, chlorides and mixtures—electrical conductance, density, viscosity, and surface tension data”. In: *Journal of Physical and Chemical Reference Data* 4 (1975), pp. 871–1178.

[29] L. Martinez et al. “PACKMOL: A package for building initial configurations for molecular dynamics simulations”. In: *Journal of computational chemistry* 30 (2009), pp. 2157–2164.

[30] V. N. Desyatnik et al. “Density, surface tension, and viscosity of uranium trichloride-sodium chloride melts”. In: *Soviet Atomic Energy* 39 (1975), pp. 649–651.

[31] G. Wang et al. “Ab-Initio Molecular Dynamics Simulations of Binary NaCl-$ThCl_4$ and Ternary NaCl-$ThCl_4$-UCl_3 Molten Salts”. In: *Journal of Molecular Liquids* 385 (2023), p. 122347.

[32] P. J. Mitchell and D. Fincham. “Shell model simulations by adiabatic dynamics”. In: *J. Phys.: Condens. Matter* 5 (1993), pp. 1031 –1038.

[33] K. Fajans and G. Joos. “Molrefraktion von Ionen und Molekülen im Lichte der Atomstruktur”. In: *Zeitschrift für Physik* 23 (1924), pp. 1 –46.

[34] R. A. Buckingham. “The classical equation of state of gaseous helium, neon and argon”. In: *Proc. Royal Soc. London. Series A, Math. Phys. Sci.* 168 (1938), pp. 264 –283.

[35] S. Grimme. “Semiempirical GGA-type density functional constructed with a long-range dispersion correction”. In: *J. Comput. Chem.* 27 (2006), pp. 1787 –1799.

[36] G. Henkelman, A. Arnaldsson, and H. Jonsson. “A fast and robust algorithm for Bader decomposition of charge density”. In: *Comput. Mater. Sci.* 36 (2006), pp. 354 –360.

[37] S. Plimpton. “Fast parallel algorithms for short-range molecular dynamics”. In: *J. Comput. Phys.* 117 (1995), pp. 1 –19.

[38] G. J. Janz et al. *Physical Properties Data Compilations Relevant to Energy Storage. II. Molten Salts: Data on Single and Multi-Component Salt Systems*. Tech. rep. National Standard Reference Data System, National Bureau of Standards, 1979.

[39] K. Grjotheim et al. “Densities and excess molar volumes of binary and ternary melts of $MgCl_2$, $CaCl_2$ and AlkCl”. In: *Trans. Faraday Soc.* 67 (1971), pp. 640 –648.

[40] E. R. Van Artsdalen and I. S. Yaffe. “Electrical conductance and density of molten salt systems: KCl–LiCl, KCl–NaCl and KCl–KI”. In: *J. Phys. Chem.* 59 (1955), pp. 118 –127.

[41] A. D. Kirshenbaum et al. “The density of liquid NaCl and KCl and an estimate of their critical constants together with those of the other alkali halides”. In: *J. Inorg. Nucl. Chem.* 24 (1962), pp. 1287 –1296.

[42] D. Dumas et al. “Theory of oscillating bodies and its utilization for determination of high-temperature viscosities”. In: *Acta Chem. Scand.* 24 (1970), pp. 510 –530.

[43] W. Brockner, K. Torklep, and H. A. Oye. “Viscosity of molten alkali chlorides”. In: *J. Chem. Eng. Data* 26 (1981), pp. 250 –253.

[44] M. Wakao, K. Minami, and A. Nagashima. “Viscosity measurements of molten LiCl in the temperature range 886-1275 K”. In: *Int. J. Thermophys.* 12 (1991), pp. 223 –230.

[45] A. B. Faheem and K. K. Lee. “Atomwise force fields for molten alkali chlorides (LiCl and KCl) and their mixtures: efficient parameterization via genetic algorithms”. In: *J. Nucl. Mater.* 573 (2023), p. 154107.

[46] O. J. Kleppa and F. G. McCarty. “Thermochemistry of charge-unsymmetrical binary fused halide Systems. II. Mixtures of magnesium chloride with the alkali chlorides and with silver chloride”. In: *J. Phys. Chem.* 70 (1966), pp. 1249 –1255.

[47] M. T. Nguyen et al. “Ab initio molecular dynamics assessment of thermodynamic and transport properties in (K,Li)Cl and (K, Na)Cl molten salt mixtures”. In: *J. Mol. Liq.* 326 (2021), p. 115262.

[48] K. Duemmler et al. “Evaluation of thermophysical properties of the LiCl-KCl system via ab initio and experimental methods”. In: *J. Nucl. Mater.* 559 (2022), p. 153414.

[49] L. Hao, S. Sridar, and W. Xiong. “Thermodynamic description of molten salt systems: KCl-LiCl-NaCl and KCl-LiCl-$NdCl_3$”. In: *J. Mol. Liq.* 382 (2023), p. 121869.

[50] G. J. Janz and R. P. T. Tomkins. *Physical Properties Data Compilations Relevant to Energy Storage. IV. Molten Salts: Data on Additional Single and Multi-Component Salt Systems*. Tech. rep. National Standard Reference Data System, National Bureau of Standards, 1981.

[51] J. Moon et al. “Density measurements of various molten sodium, magnesium, potassium, and uranium chloride salt compositions using neutron imaging”. In: *Ind. Eng. Chem. Res.* 61 (2022), pp. 17665 –17673.

[52] X. Xu et al. “Experimental test of properties of KCl–$MgCl_2$ eutectic molten salt for heat transfer and thermal storage fluid in concentrated solar power systems”. In: *J. Sol. Energy Eng.* 140 (2018), p. 051011.

[53] R. P. Clark. “Heats of fusion and heat capacities of lithium chloride-potassium chloride eutectic and potassium nitrate”. In: *J. Chem. Eng. Data.* 18 (1973), pp. 67 –70.

[54] X. Li et al. “Unrevealing the thermophysical properties and microstructural evolution of $MgCl_2$-NaCl-KCl eutectic: FPMD simulations and experimental measurements”. In: *Sol. Energy Mater. Sol. Cells* 210 (2020), p. 110504.

[55] M. H. Brooker. “A Raman spectroscopic study of the structural aspects of K_2MgCl_4 and Cs_2MgCl_4 as solid single crystals and molten salts”. In: *J. Chem. Phys.* 63 (1975), pp. 3054 –3061.

[56] G. Mohan et al. “Thermo-economic analysis of high-temperature sensible thermal storage with different ternary eutectic alkali and alkaline earth metal chlorides”. In: *Solar Energy* 176 (2018), pp. 350 –357.